The Astrophysical Journal, 681:771–797, 2008 July 10

THE FORMATION OF THE FIRST STARS. II. RADIATIVE FEEDBACK PROCESSES AND IMPLICATIONS FOR THE INITIAL MASS FUNCTION

Christopher F. McKee[1] and Jonathan C. Tan[2]
Received 2007 November 8; accepted 2008 January 23

ABSTRACT

We consider the radiative feedback processes that operate during the formation of the first stars. (1) Photodissociation of H_2 in the local dark matter minihalo occurs early in the growth of the protostar but does not affect subsequent accretion. (2) Lyα radiation pressure acting at the boundary of the H II region that the protostar creates in the accreting envelope reverses infall in the polar directions when the star reaches $\sim$20–30 $M_\odot$ but cannot prevent infall from other directions. (3) Expansion of the H II region beyond the gravitational escape radius for ionized gas occurs at masses $\sim$50–100 $M_\odot$. However, accretion from the equatorial regions can continue since the neutral accretion disk shields a substantial fraction of the accretion envelope from direct ionizing flux. (4) At higher stellar masses, $\sim$140 $M_\odot$ in the fiducial case, photoevaporation-driven mass loss from the disk, together with declining accretion rates, halts the increase in the protostellar mass. We identify this process as the mechanism that determines the mass of Population III.1 stars (i.e., stars with primordial composition that have not been affected by prior star formation). The initial mass function of these stars is set by the distribution of entropy and angular momentum. The Appendix gives approximate solutions to a number of problems relevant to the formation of the first stars: the effect of Rayleigh scattering on line profiles in media of very large optical depth, the intensity of Lyα radiation in very opaque media, radiative acceleration in terms of the gradient of a modified radiation pressure, the flux of radiation in a shell with an arbitrary distribution of opacity, and the vertical structure of an accretion disk supported by gas pressure with constant opacity.

Subject headings: cosmology: theory — early universe — stars: formation

Online material: color figures

1. INTRODUCTION

There has been substantial recent progress in our theoretical understanding of how the first stars formed (Bromm & Larson 2004). In marked contrast to the case for contemporary star formation, the initial conditions for the formation of the first stars are believed to be relatively well understood: they are determined by the growth of small-scale gravitational instabilities from cosmological fluctuations in a cold dark matter universe. The first stars are expected to form at redshifts $z \sim 10$–50 in dark matter halos of mass $\sim 10^6\ M_\odot$ (Tegmark et al. 1997). In the absence of any elements heavier than helium (other than trace amounts of lithium) the chemistry and thermodynamics of the gas are very simple (Abel et al. 2002, hereafter ABN02; Bromm et al. 2002). There are no dust grains to couple the gas to radiation emitted by the protostar. There are no previous generations of stars to roil the gas out of which the stars form, nor is there any radiation other than the cosmic background radiation. Existing calculations have assumed that there were no significant primordial magnetic fields, thereby eliminating a major complication that occurs in contemporary star formation. However, even in the absence of significant primordial fields, it is possible that magnetic fields could have been generated in the accretion disk surrounding a primordial protostar (Tan & Blackman 2004), although even in this case the magnetic fields become dynamically important only after the star formation process is well underway, and they do not affect the initial conditions. Given this relative simplicity, there is some confidence in the results of numerical simulations that have followed the collapse of cosmological scale perturbations down to almost stellar dimensions (ABN02; Bromm et al. 1999; Yoshida et al. 2006; O'Shea & Norman 2007). This confidence is strengthened by the fact that it appears to be the microphysics of H_2 cooling that determines the types of baryonic structures that are formed, and not, for example, the details of the initial power spectrum of fluctuations in dark matter density. The results of these simulations suggest that the initial gas cores out of which stars form are quite massive, $M_{\rm core} \sim 100$–1000 $M_\odot$.

The observational imprint of the first stars depends on their mass: these stars were likely to be of critical importance in reionizing the universe, in producing the first metals, and in creating the first stellar-mass black holes. The number of ionizing photons emitted per baryon depends on the stellar mass for $m_* \lesssim 300\ M_\odot$ (Bromm et al. 2001). The hardness of the radiation field is also sensitive to the mass (e.g., Tumlinson & Shull 2000; Schaerer 2002), so that He reionization can be affected. The effectiveness of the first stars in enriching the intergalactic medium (IGM) with metals and in producing the first stellar-mass black holes also depends sensitively on the mass of the star. A potential simplification in assessing these effects is that massive primordial stars are thought to have much smaller mass-loss rates than contemporary massive stars (Kudritzki 2002), so that the mass at core collapse should be quite similar to the initial mass. However, Meynet et al. (2006) have argued that if rotation is allowed for, then mass loss can be significant. Heger & Woosley (2002) showed that stars exploding as supernovae above about 260 $M_\odot$ and between 40 and 140 $M_\odot$ should collapse directly to black holes, and they argued that such stars would provide relatively little metal enrichment. However, Ohkubo et al. (2006) followed the collapse and explosion of 500 and 1000 $M_\odot$ stars in two dimensions and concluded that a substantial amount of metals could be ejected; they proposed that such supernovae could produce intermediate-mass black holes. Heger & Woosley (2002) also showed that for

[1] Departments of Physics and Astronomy, University of California, Berkeley, CA 94720; cmckee@astro.berkeley.edu.
[2] Department of Astronomy, University of Florida, Gainesville, FL 32611; jt@astro.ufl.edu.

140 $M_\odot \lesssim m_* \lesssim 260\ M_\odot$, the pair instability leads to explosive O and Si burning that completely disrupts the star, leaving no remnant and ejecting large quantities of heavy elements. Such supernovae produce a dramatic odd-even effect in the nuclei produced. Stars below $\sim 40\ M_\odot$ are expected to form neutron stars, with more normal enrichment rates. In principle, metallicity determinations from high-redshift absorption-line systems (Schaye et al. 2003; Norman et al. 2004) or from very metal-poor local stars (Beers & Christlieb 2005) can constrain the initial mass function (IMF) of the early generations of stars. Indeed, based on observations such as these, Daigne et al. (2004) argue that the stars responsible for reionizing the universe mostly likely had masses $\lesssim 100\ M_\odot$, and Tumlinson (2006) concludes that stars above 140 $M_\odot$ could have contributed at most 10% of the iron observed in extremely metal-poor stars (those with [Fe/H] $< 10^{-3}$; Beers & Christlieb 2005).

In discussing the formation of the first stars, the terms "first stars" and "Population III stars" are often used interchangeably, but this can lead to confusion. To be precise, we follow the conventions suggested by one of us at the First Stars III conference (O'Shea et al. 2008) and define Population III stars as those stars with a metallicity sufficiently low that it has no effect on either the formation or the evolution of the stars. The value of the critical metallicity for star formation, i.e., the value below which the metals do not influence star formation, is uncertain, with estimates ranging from $\sim 10^{-6}\ Z_\odot$ if the cooling is dominated by small dust grains that contain a significant fraction of the metals (Omukai et al. 2005) to $\sim 10^{-3.5}\ Z_\odot$ if the cooling is dominated by the fine-structure lines of C and O and there is negligible H_2 (Bromm & Loeb 2003); if H_2 cooling is included, Jappsen et al. (2007) argue that there is no critical metallicity for gas-phase metals. It is possible that values of the metallicity even less than $10^{-6}\ Z_\odot$ could significantly affect the evolution of primordial stars (G. Meynet 2007, private communication). Among Population III stars, we distinguish between the first and second generations, termed Population III.1 and III.2, respectively: the initial conditions for the formation of Population III.1 stars are determined solely by cosmological fluctuations, whereas those for Population III.2 stars are significantly affected by other stars. It is likely that Population III.1 stars have a primordial composition, since it is hard to see how the gas out of which they form could be contaminated by even trace amounts of metals without having been affected by radiation from the star that produced the metals. Stars affect the initial conditions for the formation of Population III.2 stars primarily by radiation, both ionizing radiation and Lyman-Werner band radiation that destroys H_2 molecules. The latter reduces the cooling efficiency of the gas, allowing compression to heat up to the point that it begins to become collisionally ionized; shocks associated with H II regions and supernova remnants can also ionize the gas. Once the gas has been partially ionized, HD cooling can become important, reducing the characteristic star formation mass (Uehara & Inutsuka 2000). Greif & Bromm (2006) use the term "Population II.5" to describe stars that form from gas in which HD cooling is important, whereas in our terminology these would be Population III.2 stars, but we believe that it is better to describe all essentially metal-free stars as "Population III." It should be noted that our definition of Population III.2 stars includes all Population III stars that were significantly affected by previous generations of star formation, even if that did not result in significant HD production. Those Population III.2 stars that form out of gas that is enriched in HD will typically be less massive than Population III.1 stars, by about a factor of 10 according to Greif & Bromm (2006). They infer that Population III.1 stars are relatively rare, constituting about 10% by mass of all Population III stars.

In this paper we wish to estimate the characteristic mass of the first generation of stars (Population III.1). Even if they are relatively rare, they are critical in setting the initial conditions for the star formation that followed and therefore in determining the reionization of the universe and the production of the first metals and the first stellar-mass black holes. For contemporary star formation, it is believed that the IMF is set by a combination of gravitational fragmentation in a turbulent medium (Elmegreen 1997; Padoan & Nordlund 2002) and feedback effects. The characteristic stellar mass is of order the Bonnor-Ebert mass, $m_{\rm BE} \propto T^{3/2}/\rho^{1/2}$. However, not all of the initial core mass is incorporated into the final star, since contemporary protostars have powerful outflows that eject some of the core mass (Nakano et al. 1995; Matzner & McKee 2000). There are a number of feedback effects that occur in contemporary massive star formation (Larson & Starrfield 1971), particularly radiation pressure on dust and photoionization associated with the growth of an H II region. It remains unclear whether the upper limit on the contemporary IMF is set by feedback or by instabilities that afflict very massive stars.

The clumps out of which the first stars form have total masses, including dark matter, of order $10^6\ M_\odot$; these objects are typically referred to as minihalos. Cooling by trace amounts of H_2 generally leads to the formation of a gravitationally unstable core of baryonic mass $\sim 10^2$–$10^3\ M_\odot$ (ABN02). In contrast to contemporary star-forming regions, the turbulence in this gas is subsonic, due to the higher temperatures and the lack of internal and external sources of turbulence. As a result, gravitational fragmentation is much less effective: indeed, numerical simulations show no evidence for it (e.g., ABN02; Yoshida et al. 2006; but see Clark et al. 2008), and analytic calculations (Ripamonti & Abel 2004), including those that consider disk fragmentation (Tan & Blackman 2004), show no evidence for fragmentation either. It therefore appears that the mass of the first stars is likely to be set by feedback effects.

Feedback effects can be classified as either radiative or kinetic. Kinetic feedback includes protostellar outflows and main-sequence winds. In contemporary star formation, outflows are believed to be hydromagnetically driven; in this paper we assume that the magnetic fields associated with the protostar are too weak or too tangled to drive a strong outflow (for a more extensive discussion of the effect of these outflows see Tan & Blackman 2004). Due to the absence of metals, main-sequence winds are very weak in the absence of rotation (Kudritzki 2002), although they could become important in the later stages of evolution if the star is rapidly rotating. Since we are primarily interested in the early stages of evolution of the star, we neglect kinetic feedback (i.e., outflows and winds).

Radiative feedback includes radiation pressure, photoionization heating, and photodissociation. Radiation pressure can be due to continuum radiation or to resonance line scattering; the continuum radiation pressure can be due to electron scattering or to photoionization. Photoionization also leads to heating, which unbinds gas beyond the gravitational radius $r_g \equiv Gm_*/c_s^2$, where c_s is the isothermal sound speed of the gas. If the gas is initially in a disk, this process is termed photoevaporation. Finally, photodissociation destroys H_2, the dominant coolant in neutral primordial gas.

Most previous work has focused on the effects of continuum radiation pressure and photoionization heating in limiting the mass of primordial stars. Omukai & Palla (2001, 2003) focused on electron scattering, which leads to the Eddington limit on an accreting mass. For the case of spherical accretion at a rate of $4.4 \times 10^{-3}\ M_\odot\ {\rm yr}^{-1}$, radiation pressure first becomes important at around 80 $M_\odot$, leading to a dramatic swelling of the stellar surface. This, however, is a transient effect because an important part of the luminosity is due to accretion, which is reduced by the

increase in the stellar radius. Only at masses around 300 $M_\odot$ does the internal luminosity become very close to the Eddington value, leading to runaway expansion of the star and, presumably, the end of accretion. Omukai & Palla (2003) considered a range of accretion rates. They found that if the accretion rate is smaller than $4.4 \times 10^{-3}\ M_\odot\ \mathrm{yr}^{-1}$, then the total luminosity remains sub-Eddington and the star continues to grow along the main sequence to arbitrarily large masses. On the other hand, if the accretion rate is somewhat larger than this critical rate, the Eddington limit becomes important at around 100 $M_\odot$. Accretion at a rate based on the settling motions in the core of ABN02 is slow enough that the Eddington limit does not affect the final mass. However, these models ignored the influence of other protostellar feedback mechanisms on the infalling envelope. These models also assumed spherical symmetry, which leads to much larger photospheric radii and thus a softer radiation field than in the more realistic case of disk accretion (see § 7 in Tan & McKee 2004, hereafter Paper I).

Omukai & Inutsuka (2002) considered the combined effects of photoionization heating and continuum radiation pressure due to photoionization in the infalling envelope. They show that there is a critical stellar mass at which the hydrogen-ionizing luminosity is sufficient to create an H II region, which rapidly spreads to large distances where its thermal pressure becomes dynamically important in slowing infall. However, the ionizing radiation force decelerates the inflowing gas, raising the gas density and therefore reducing the radius of the H II region. For spherical inflow, this mechanism is so effective that the radius of the H II region remains well below the gravitational radius r_g, stopping any mass loss. They concluded that with this effect, there was no limit on protostellar masses below 1000 $M_\odot$. Without this radiation force, they predicted a mass limit of order 300 $M_\odot$. As seen below, these conclusions are sensitive to the assumption of spherical accretion.

In Paper I we modeled the growth of a primordial protostar from very small to large masses. We included the effects of rotation of the infalling gas, which led to the formation of an accretion disk around the protostar. The goal of this paper is to determine when the energy output from the protostar is sufficient to halt accretion and set the final stellar mass. This is an extremely complicated problem, the full solution of which requires three-dimensional hydrodynamical simulations that include the generation, propagation, and dynamical influence of radiation. Furthermore, these simulations must resolve a large range of scales: the protostar is of order 10 $R_\odot$, while the size of the quasi-hydrostatic core that encloses $\sim$1000 $M_\odot$ is of order 1 pc, several million times greater. The demands on the timescale are even greater: the simulation may have to follow the evolution of the star over its lifetime $\sim$2–3 Myr (Schaerer 2002) while at the same time following the dynamics of an accretion disk with a characteristic timescale as short as 10^4 s. The numerical simulations of ABN02 were able to resolve an even greater range of radii, but it will be some years before it is possible to meet the required dynamical range in timescales. As a result, we shall develop simple analytic models for the feedback interaction that we hope will provide a useful first step.

We begin our discussion with a review of the results of Paper I in § 2. Feedback effects are then considered in the approximate order in which they become manifest. In § 3 we briefly discuss the effects of photodissociation. Lyα radiation pressure feedback is considered in § 4 and in several appendices. The feedback from ionizing photons that can create an H II region is considered in § 5. After discussing shadowing by accretion disks in § 6 and an appendix, the feedback due to disk photoevaporation is considered in § 7. Figure 1 gives an overview of these feedback processes occurring near the protostar. Finally, our conclusions are summarized in § 8.

2. REVIEW OF PAPER I: PROPERTIES AND EVOLUTION OF PRIMORDIAL PROTOSTARS

The radiative output from a protostar depends on the temperature and luminosity of its emitting components, which are the star itself (stellar photosphere), the boundary layer of the accretion disk with the star, and the larger scale accretion disk. The luminosity of the star depends mostly on its mass. The size of the star then determines its temperature. The size of the star and the accretion rate determine the radiative properties of both the boundary layer and the accretion disk, since emission from the latter is dominated by the inner regions.

The size of the star depends on the accretion rate during its formation history. At lower masses there is a balance in the size set by the need to radiate the luminosity, which is mostly due to accretion, with a photospheric temperature that is likely to be close to $\sim$6000 K because the opacity due to H^- rapidly declines in this temperature regime. Under the assumption of spherical accretion, Stahler et al. (1986) found the protostellar radius to be

$$r_* \simeq 90.8 m_{*,2}^{0.27} \dot{m}_{*,-3}^{0.41}\ R_\odot \quad \left(m_{*,2} \lesssim 0.1\right), \tag{1}$$

where $m_{*,2} \equiv m_*/(100\ M_\odot)$ and $\dot{m}_{*d,-3} \equiv \dot{m}_{*d}/(10^{-3}\ M_\odot\ \mathrm{yr}^{-1})$. For the accretion rates typical of primordial star formation we see that the size is very large. For more massive protostars there is a transition once the star is about as old as its local Kelvin-Helmholtz time, and then contraction proceeds toward the main-sequence size, where accretion can continue. In Paper I we found that for typical conditions, the protostar reached its main-sequence radius at about 100 $M_\odot$. According to Schaerer (2002), this radius is

$$r_* \simeq 4.3 m_{*,2}^{0.55}\ R_\odot \quad \text{(main sequence)} \tag{2}$$

to within 6% for $0.4 \leq m_{*,2} \leq 3$.

Thus, almost all the radiative stellar properties depend on just two parameters: the stellar mass and the accretion rate. Note that in principle these properties also depend on the angular momentum of the infalling gas, since if there was no rotation, then spherical accretion implies very high gas densities near the protostar, affecting the location of its photosphere. However, for any realistic amount of angular momentum, a disk forms whose size is much larger than r_*, and the star's properties no longer depend on the rotation of the core from which the star forms.

The accretion rate of Population III protostars depends on the density structure of the gas core at a point when the star starts to form. This density structure is set by the balance of thermal pressure and self-gravity, which in turn depends primarily on the cooling properties of molecular hydrogen. This cooling creates almost isothermal cores at $T \simeq 200$ K with an outer bounding density of about $10^4\ \mathrm{cm}^{-3}$, which is the critical density of H_2 cooling transitions (for H_2 molecules interacting with atomic H). In fact, the temperatures increase to several hundred kelvin in the inner parts of the core because of the reduced cooling efficiency above the critical density. These basic features have been confirmed by numerical studies (ABN02; Bromm et al. 2002; O'Shea & Norman 2007). The trigger for dynamical collapse is thought to be the rapid formation of H_2 by three-body collisions at high densities $\sim 10^{10}\ \mathrm{cm}^{-3}$, since this then dramatically increases the cooling rate in this region.

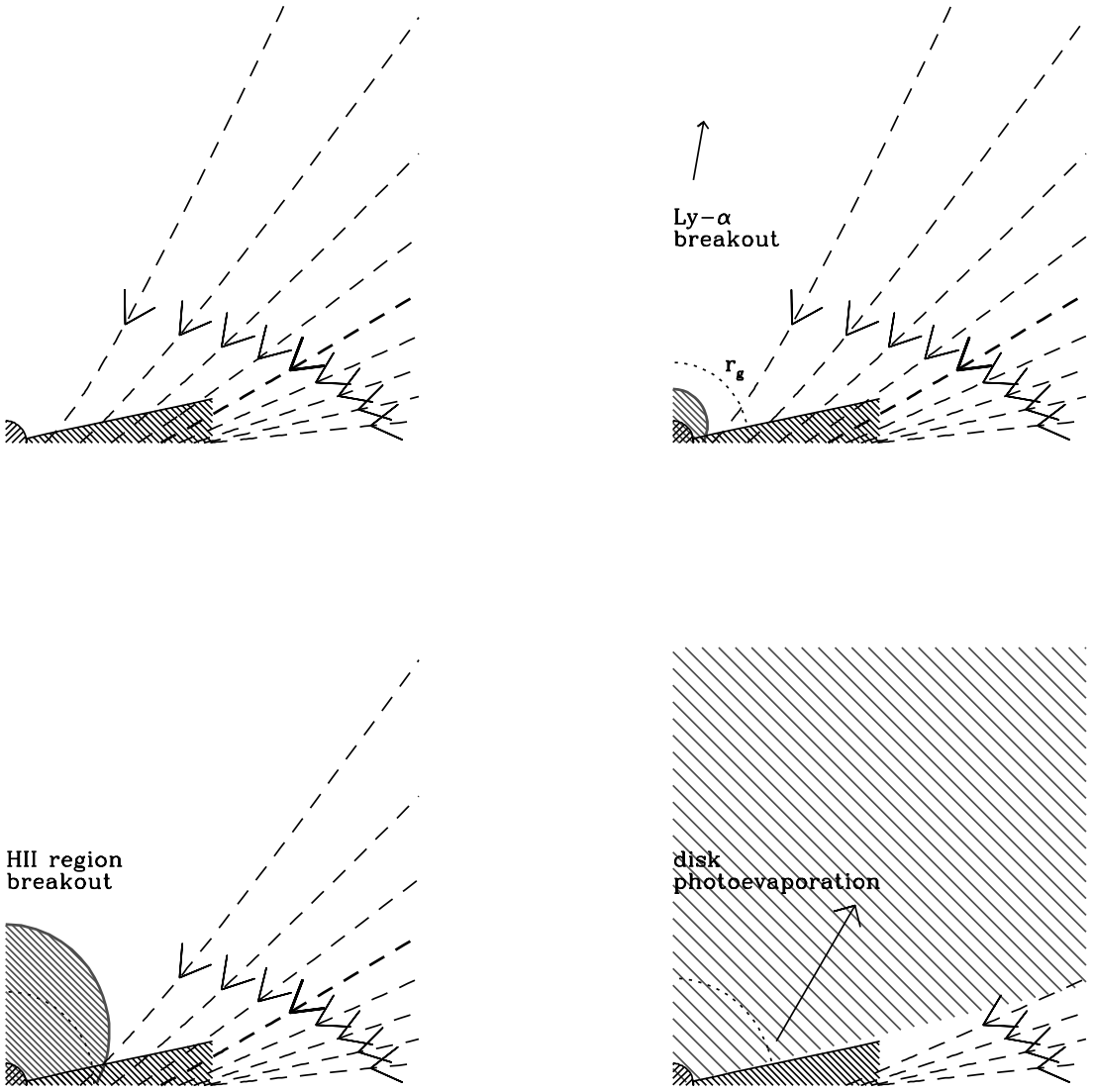

FIG. 1.—Overview of the accretion geometry and feedback processes involved in primordial star formation. *Top left*: Cross section of the accretion geometry: the dashed lines show streamlines of the rotating, infalling gas, with figure of revolution from each streamline separating 10% of the total infall from this hemisphere. The aspect ratio of the accretion disk is realistic, while the size of the star has been exaggerated for clarity. *Top right*: The shaded region around the star shows the extent of the H II region, which at this relatively early stage is still confined inside the gravitational radius for the escape of ionized gas, r_g. Lyα radiation pressure feedback should be strong enough to prevent accretion in the polar directions. *Bottom left*: The stellar mass and ionizing luminosity have grown, and the H II region is just in the process of breaking out of the accretion flow. Once a significant volume beyond r_g is ionized, accretion from these directions is expected to be shut off. *Bottom right*: Final stage of accretion involves shadowing of the equatorial region from stellar ionizing flux by the disk, which at the same time is photoevaporated. The competition between this photoevaporative outflow and the residual accretion rate sets the final mass of the star. [*See the electronic edition of the Journal for a color version of this figure.*]

ABN02 carried their calculations almost to the point of protostar formation, and at this time gas was flowing inward subsonically almost everywhere (except for $0.1\ M_\odot \lesssim M \lesssim 1\ M_\odot$, where the inflow was slightly supersonic). Shu's (1977) expansion wave solutions for protostellar accretion are based on the assumption that the inflow velocity at this time is zero. Hunter (1977) generalized these solutions and showed that there is a discrete set of self-similar solutions that begin at rest at $t = -\infty$ and have a constant infall velocity at the time of protostar formation ($t = 0$). One of these solutions, the Larson-Penston solution (Larson 1969; Penston 1969), has supersonic inflow (Mach number of 3.3 at $t = 0$); this solution is clearly inconsistent with the numerical results. In fact, the accretion flow appears to be a settling solution regulated by H_2 cooling. Only one of Hunter's solutions corresponds to mildly subsonic inflow (Mach number of 0.295 at $t = 0$), comparable to that found by ABN02, and this is the solution adopted in Paper I. This solution has a density that is 1.189 times greater than a singular isothermal sphere at $t = 0$, and the accretion rate is 2.6 times greater.

Hunter's (1977) solution applies to an isothermal gas. Omukai & Nishi (1998) and Ripamonti et al. (2002) have numerically calculated accretion rates for primordial protostars and showed that the accreting gas is isentropic with an adiabatic index $\gamma \simeq 1.1$ due to H_2 cooling; i.e., each mass element satisfies the relation $P = K\rho^\gamma$ with the "entropy parameter" $K = \text{const}$. In hydrostatic equilibrium, such a gas settles into a polytropic configuration, which in general has $P(r) = K_p\rho(r)^{\gamma_p}$. For an isentropic gas, we have $\gamma_p = \gamma$ and $K_p = K$. In Paper I we presented an analytic model for the protostellar accretion rate for isentropic gas. We allowed for the existence of an accretion disk around the protostar with a significant fraction of the stellar mass,

$$m_{*d} = m_* + m_d \equiv (1 + f_d)m_*, \tag{3}$$

with a fiducial value for the disk mass fraction $f_d = \frac{1}{3}$. Following McKee & Tan (2002, 2003), we wrote the accretion rate as

$$\dot{m}_{*d} = \phi_* \frac{m_{*d}}{t_{\rm ff}}, \tag{4}$$

where ϕ_* is a numerical constant of order unity and $t_{\rm ff} = (3\pi/32G\rho)^{1/2}$ is the free-fall time of the gas (measured at $t = 0$). For gas that is in hydrostatic equilibrium at $t = 0$, McKee & Tan (2002) showed that $\phi_* \simeq 1.62 - 0.96/(2 - \gamma_p)$ to within about 1% for $0 < \gamma_p \leq 1$; we have since verified that this is valid for $\gamma_p \lesssim 1.2$. To our knowledge, Hunter's self-similar solutions starting at $t = -\infty$ have not been generalized to the nonisothermal case.[3] In Paper I we therefore assumed that the accretion rate for the $\gamma = 1$ case is 2.6 times greater than that for hydrostatic initial conditions, just as in the isothermal case.

Feedback from the star, whether due to winds, photoionization, or radiation pressure, can reduce the accretion rate onto the star. We define a hypothetical star-disk mass, $m_{*d,0}$, and accretion rate, $\dot{m}_{*d,0}$, in the absence of feedback. In this case, the star-disk mass equals the mass of the core out of which it was formed, $m_{*d,0} = M(r)$. The instantaneous and mean star formation efficiencies are

$$\epsilon_{*d} \equiv \frac{\dot{m}_{*d}}{\dot{m}_{*d,0}}, \tag{5}$$

$$\bar{\epsilon}_{*d} \equiv \frac{m_{*d}}{m_{*d,0}} = \frac{m_{*d}}{M}. \tag{6}$$

In our previous work, we assumed that the star formation efficiency was constant, so that $\epsilon_{*d} = \bar{\epsilon}_{*d}$. In the present work, we find that significant feedback does not set in until the star is fairly massive, so that we must distinguish the instantaneous and mean values. In Paper I we found that the accretion rate onto the star-disk system is

$$\dot{m}_{*d} = 0.026 \left[\frac{\epsilon_{*d} K'^{15/7}}{(M/M_\odot)^{3/7}} \right] M_\odot \ {\rm yr}^{-1}, \tag{7}$$

where

$$K' \equiv \frac{P/\rho^\gamma}{1.88 \times 10^{12} \ {\rm cgs}} = \left(\frac{T'_{\rm eff}}{300 \ {\rm K}} \right) \left(\frac{10^4 \ {\rm cm}^{-3}}{n_{\rm H}} \right)^{0.1} \tag{8}$$

is a measure of the entropy of the accreting gas. Here $T'_{\rm eff} \equiv T + \mu\sigma^2_{\rm turb}/k$ is an effective temperature that includes the effect of turbulent motions; we have added a prime to the $T_{\rm eff}$ defined in Paper I to distinguish it from the effective temperature of a radiating atmosphere. Expressing the accretion rate in terms of the stellar mass, which equations (3) and (6) imply is $m_* = \bar{\epsilon}_{*d} M/(1 + f_d)$, we find

$$\dot{m}_{*d} = 0.026 \left[\frac{\epsilon_{*d} \bar{\epsilon}_{*d}^{3/7} K'^{15/7}}{(1 + f_d)^{3/7} (m_*/M_\odot)^{3/7}} \right] M_\odot \ {\rm yr}^{-1}. \tag{9}$$

With $K' = \epsilon_{*d} = \bar{\epsilon}_{*d} = 1$, this result is in good agreement with the results of Omukai & Nishi (1998) and Ripamonti et al. (2002); since their one-dimensional calculations did not allow for disks, this comparison is made for $f_d = 0$. Note that this agreement validates our use of the Hunter mildly subsonic solution to infer the accretion rate. If $\epsilon_{*d} = 1$ (i.e., no feedback) and $f_d = \frac{1}{3}$, then the accretion rate onto the star+disk is

$$\dot{m}_{*d,-3} \rightarrow 3.20 \left(\frac{K'^{15/7}}{m_{*,2}^{3/7}} \right), \tag{10}$$

where henceforth it will be understood that numerical evaluations denoted by "$\rightarrow$" have $\epsilon_{*d} = 1$ and $f_d = \frac{1}{3}$. In this case the accretion rate onto the star (which may be primarily through the disk) is $\frac{3}{4}$ of this [since $\dot{m}_* = \dot{m}_{*d}/(1 + f_d)$].

Our estimate of the accretion rate is somewhat above that estimated by ABN02, but this is to be expected since their calculation stopped prior to the formation of the protostar. Indeed, at the time at which the protostar first forms ($t = 0$), the accretion rate at any finite radius r [i.e., $\dot{m}(r) = 4\pi r^2 \rho |v_r|$] in a self-similar, isothermal collapse is smaller than the value it has at times $t > r/c_s$, where c_s is the isothermal sound speed. Equivalently, at a given time, the accretion rate at radii $r \gtrsim c_s t$ is less than that at small radii, $r \ll c_s t$. In the Shu (1977) solution for the collapse of a singular isothermal sphere, the accretion rate at a given time is zero outside the expansion wave at $r = c_s t$; inside the expansion wave, the accretion rate smoothly increases to $0.975 c_s^3/G$ as $r \rightarrow 0$. For the Larson-Penston solution, the accretion rate at a given time $t > 0$ increases from $29 c_s^3/G$ at large radii ($r \gg c_s t$) to $47 c_s^3/G$ at small radii ($r \ll c_s t$). For Hunter's mildly subsonic solution, which we have suggested is closest to the numerical simulations, the accretion rate increases from $0.70 c_s^3/G$ at large radii to $2.58 c_s^3/G$ at small radii (Hunter 1977), an increase of a factor of 3.7. This demonstrates that caution should be exercised in inferring accretion rates at late times from those measured at early times, which is commonly done in simulations (e.g., ABN02; Yoshida et al. 2006; O'Shea & Norman 2007).

The age of the star when it reaches a mass m_* is (Paper I)

$$t_{\rm yr} = 27 \left(\frac{1 + f_d}{\bar{\epsilon}_{*d}} \right)^{10/7} K'^{-15/7} \left(\frac{m_*}{M_\odot} \right)^{10/7} \rightarrow 2.92 \times 10^4 K'^{-15/7} m_{*,2}^{10/7}, \tag{11}$$

where $t_{\rm yr} \equiv t/(1 \ {\rm yr})$ and where it is the mean star formation efficiency $\bar{\epsilon}_{*d}$ that enters. The resulting stellar mass is

$$m_* \rightarrow 0.075 K'^{1.5} t_{\rm yr}^{0.7} \ M_\odot. \tag{12}$$

Bromm & Loeb (2004) have carried out a three-dimensional simulation of the accretion onto the protostar for the first 10^4 yr, and for $K' = 1$ our result is within a factor of $\sim$2 of theirs for this time period. (However, it should be noted that an extrapolation of their result to times beyond 5×10^4 yr gives a mass less than half our estimate of the mass of the star plus disk. It remains to be determined whether such an extrapolation is valid.)

[3] Fatuzzo et al. (2004) have given a comprehensive discussion of self-similar accretion solutions that start at $t = 0$, allowing for inflow velocity, overdensity relative to hydrostatic equilibrium, and nonisentropic gas ($\gamma \neq \gamma_p$). Although they do not treat the time prior to protostar formation, their isothermal results for $t > 0$ are consistent with Hunter's, as expected. For the nonisothermal case, Fatuzzo et al. (2004) present results for gas that is inflowing at $r \rightarrow \infty$, but these are not self-similar in that the accretion rate depends on where the integration begins (F. Adams 2004, private communication). However, it is possible to generalize their treatment so that the Mach number of the inflow is constant. Presumably the overdensity and infall Mach number of the $\gamma = 1.1$ analog of the mildly subsonic Hunter solution are similar to those of the isothermal solution; if they are exactly the same, then the accretion rate would be about 2.0 times that for the case of hydrostatic initial conditions, somewhat less than the isothermal value of 2.6.

With this estimate of the protostellar mass, it is possible to calculate the maximum possible mass a primordial star could have. Schaerer (2002) has calculated the main-sequence lifetimes of primordial stars with no mass loss for $m_* \leq 500\ M_\odot$, and his results are accurately described by the expression $t_{\rm ms} \simeq 2.7 m_{*,2}^{-0.24}$ Myr for $100\ M_\odot \lesssim m_* \lesssim 500\ M_\odot$. If we assume that the accretion is not limited by any feedback processes ($\epsilon_{*d} = 1$), that Schaerer's results can be extrapolated to higher masses, and that accretion during the relatively short post–main-sequence phase is negligible, then we find

$$m_{*,\max} = \int_0^{t_{\rm ms}} \dot{m}_*\, dt \simeq 1900 \left(\frac{1}{1+f_d}\right)^{0.86} K'^{1.28}\ M_\odot \rightarrow 1500 K'^{1.28}\ M_\odot. \quad (13)$$

The maximum possible stellar mass is thus controlled by the value of the entropy parameter of the core.

In Paper I we also considered the effect of rotation. Rotation of the infalling gas has a dramatic effect on the evolution of the protostar, since it leads to much smaller photospheric radii and correspondingly higher temperatures and accretion luminosities. We parameterized the rotation in terms of

$$f_{\rm Kep} \equiv \frac{v_{\rm rot}(r_{\rm sp})}{v_{\rm Kep}(r_{\rm sp})}, \quad (14)$$

the ratio of the rotational velocity to the Keplerian velocity measured at the sonic point at $r_{\rm sp}$. ABN02 found $f_{\rm Kep} \sim 0.5$ independent of radius, so we adopt this as a fiducial value. We then showed that the accreting gas formed a disk with an outer radius

$$r_d = 1.92 \times 10^{16} \left(\frac{f_{\rm Kep}}{0.5}\right)^2 \left(\frac{m_{*d,2}}{\bar{\epsilon}_{*d}}\right)^{9/7} K'^{-10/7}\ {\rm cm} \quad (15)$$

$$\rightarrow 2.78 \times 10^{16} \left(\frac{f_{\rm Kep}}{0.5}\right)^2 \frac{m_{*,2}^{9/7}}{K'^{10/7}}\ {\rm cm}. \quad (16)$$

3. PHOTODISSOCIATION FEEDBACK

As the protostar grows in mass, it begins to emit copious amounts of nonionizing ultraviolet radiation (far-ultraviolet [FUV] radiation), as shown in Figure 2. This radiation can photodissociate the H_2 that is critical for cooling the accreting gas (Omukai & Nishi 1999; Glover & Brand 2001); its dynamical effects are considered in the next section.

Once the molecular coolants in the accreting gas are destroyed, the adiabatic index rises from $\gamma \simeq 1.1$ to $\gamma = 5/3$. If the gas were able to continue contraction, it would heat up until the temperature became high enough ($T \sim 10^4$ K) to excite the Lyα transition. For $T \gtrsim 10^4$ K, the adiabatic index would then drop back to about 1.

Can the protostar continue to accrete when $\gamma \simeq 5/3$? If one considers the related problem of the gravitational stability of polytropic gas spheres, one might be led to conclude that accretion would stop: polytropic stars are stable against gravitational collapse for $\gamma > 4/3$ (Shapiro & Teukolsky 1983, p. 145), and the same is true for polytropic gas clouds even if $\gamma_p < 4/3$ (McKee & Holliman 1999). However, there is a crucial distinction between collapse onto a protostar and the contraction of a gas cloud prior to protostar formation, and that is the presence of the central protostar, which is effectively a mass singularity. The stability analyses cited above assumed that there was no mass singularity at the origin. When one is present, the problem is analogous to that of Bondi accretion, the accretion of non–self-gravitating gas onto a star; this can occur for $\gamma = 5/3$ (e.g., Shapiro & Teukolsky 1983, pp. 412–420). The problem of protostellar accretion, which includes the self-gravity of the gas, has been considered by Fatuzzo et al. (2004) for a wide range of conditions. They showed that gravity dominates over pressure close to the protostar, so that accretion can occur, provided that $\gamma < 5/3$. It is straightforward to see why: in supersonic inflow, the density scales as $\rho \propto r^{-3/2}$, so that the temperature $T \propto r^{-3(\gamma-1)/2}$ rises more slowly than the kinetic energy per unit mass $\propto r^{-1}$ provided that $\gamma < 5/3$. They demonstrated that the accretion rate for a singular, initially isothermal sphere with $\gamma = 1.6$ is only slightly smaller than for the case in which $\gamma = 1$.

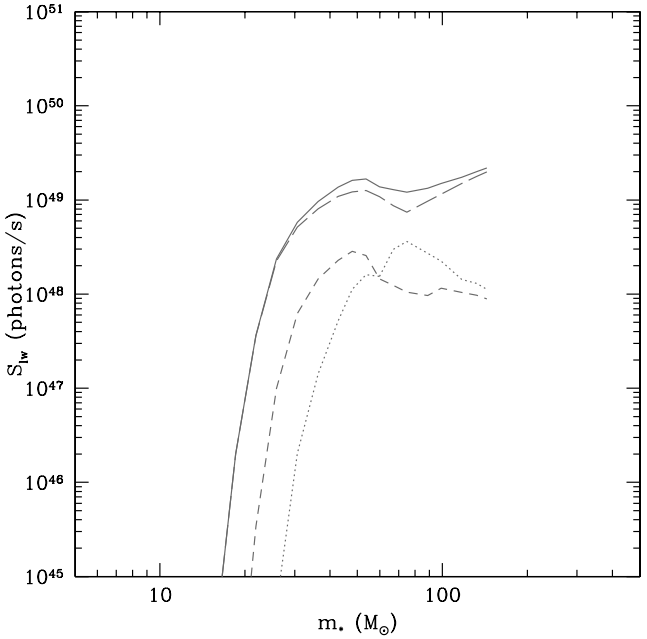

FIG. 2.—Evolution of Lyman-Werner photon luminosity from the fiducial model of primordial star formation, including effects of stellar feedback. The total (*solid line*) and contributions from the protostellar surface (*long-dashed line*), boundary layer (*short-dashed line*), and accretion disk from $r < 10 r_*$ (*dotted line*) are shown. [*See the electronic edition of the Journal for a color version of this figure.*]

The argument of Fatuzzo et al. (2004) applies to the inner, supersonic region of infall. What about the outer, subsonic region? There the density varies as a higher power of radius (e.g., for $v_{\rm infall} = {\rm const}$, $\rho \propto r^{-2}$), so that pressure can overcome gravity at a lower value of γ. To see this more quantitatively, consider the case of a singular isothermal sphere with $\gamma \neq 1$. Assume that the initial density of the sphere is Λ times greater than the equilibrium value. If the gas is flowing inward at a velocity $-v_\infty$ far from the protostar [i.e., at large values of the similarity variable x, which is just $r/(c_s t)$ in the isothermal case], then v varies as

$$v = -v_\infty - \frac{2(\Lambda-1)}{x} - \frac{(4-3\gamma)v_\infty}{x^2} + \ldots \quad (17)$$

(Fatuzzo et al. 2004; we have corrected a typo in the last factor). Thus, for $\gamma > 4/3$, pressure forces will tend to decelerate the flow; however, this can be overcome by a suitable overdensity Λ. We have confirmed this by numerical integration of the equations given by Fatuzzo et al. (2004): for $v_\infty > 0$ and $\gamma \leq 4/3$, accretion is possible for $\Lambda \geq 1$; for $5/3 \geq \gamma > 4/3$, accretion is possible provided that Λ exceeds some threshold. For primordial star formation, we estimate $\gamma_p = 1.1$ and $v_\infty/c_s \simeq 0.3$–0.5; accretion can occur in this case for $\gamma = 5/3$ for $\Lambda > 1.16$ and 1.28,

respectively. These overdensities are quite modest (for example, the Hunter [1977] subsonic infall solution has $v_\infty/c_s = 0.295$ and $\Lambda = 1.189$), so we anticipate that photodissociation should not prevent protostellar accretion. The value of the overdensity is likely to vary from one protostar to another, however, so it is possible that in some cases it would be too small to permit accretion. In such cases the infalling gas would decelerate; once it is stationary, however, it could resume accretion when it is overtaken by an expansion wave, as shown by Fatuzzo et al. (2004). Our numerical calculations show that the increase in γ from 1.1 to 5/3 has only a minor effect on the accretion rate, diminishing it by less than 20%. We conclude that photodissociation of molecular coolants by the protostar does not have a significant effect on its accretion rate.

On the other hand, collapsing cores that do not contain a protostar, but that are close enough to a protostar that their molecular coolants are destroyed, will cease collapsing if their central temperature is low enough ($<10^4$ K) that γ exceeds 4/3. Thus, FUV emission from the first stars is potentially quite effective at suppressing star formation in their vicinity. We can estimate the distance over which star formation is suppressed from the work of Glover & Brand (2001). As in Paper I, we assume that the core is in approximate hydrostatic equilibrium and is characterized by an entropy parameter K. We find that the time to dissociate H_2 is less than the free-fall time $t_{\rm ff}$ if the core is within a distance

$$D = 24\left[\left(\frac{S_{\rm LW}}{10^{49}\ {\rm s}^{-1}}\right)\left(\frac{10^{-3}}{x_2}\right)\left(\frac{f_{\rm abs}\,f_{\rm diss}}{0.01}\right)\right]^{1/2}\frac{1}{\bar{n}_4^{21/40}K'^{1/4}}\ {\rm pc} \tag{18}$$

of the protostar, where $S_{\rm LW}$ is the photon luminosity in the Lyman-Werner bands, x_2 is the fractional abundance of H_2, $f_{\rm abs}$ is the fraction of the Lyman-Werner flux absorbed by the H_2, $f_{\rm diss}$ is the fraction of absorptions that result in dissociation, and $\bar{n}$ is the mean density of H nuclei. Thus, even a 100 $M_\odot$ star, which has $S_{\rm LW} \simeq 10^{49}\ {\rm s}^{-1}$, can suppress star formation in an existing core only if the core is relatively nearby. A more detailed analysis by Susa (2007) comes to the same conclusion. Ahn & Shapiro (2007) model both dissociation and ionizing feedback and also find a relatively weak suppression of Population III.2 star formation by neighboring Population III.1 stars. Whalen et al. (2008) have presented multidimensional numerical simulations of these processes.

4. Lyα RADIATION PRESSURE

The second feedback effect of FUV radiation is radiation pressure acting on the Lyman absorption series in the infalling neutral gas. This effect has been considered previously by Oh & Haiman (2002), who studied feedback effects in halos with virial temperatures above 10^4 K, which are more massive than those we consider. They concluded that Lyα radiation pressure could be important but did not find any constraint on the mass of the star that could form. Our work improves on theirs in several respects: we include stellar continuum photons injected away from line center, as well as Lyα photons emitted in the H II region; we allow for Rayleigh scattering; we include the limitations on the radiation pressure set by two-photon emission and by the blackbody constraint; and we allow for the effects of rotation in the infalling gas.

Since conditions are very opaque, the Lyα radiation can be considered to be isotropic. The Lyα radiation pressure is then

$$P_\alpha = \frac{1}{3}u_\alpha = \frac{4\pi J_\alpha}{3c}, \tag{19}$$

where u_α and J_α are the energy density and mean intensity of the Lyα radiation. The estimation of J_α is complicated by the fact that Lyα photons can diffuse in frequency as well as in space, and that at the optical depths we are considering, the transfer is dominated by the damping wings of the line profile (Adams 1972). This problem is far too difficult to treat analytically for the geometry and dynamics that we are using to model the protostellar accretion. We therefore make the following substantial approximations when evaluating J_α at the outer boundary of the H II region, $r_{\rm H\,II}$ (which may be at the surface of the protostar), and at a particular polar angle: (1) The axially symmetric geometry can be replaced by an equivalent slab geometry. The effects of spherical divergence are incorporated by normalizing the mean intensity to the flux at $r_{\rm H\,II}$. The slab column is set equal to 20% of that in the infalling gas based on the discussion in Appendix C. (2) The anisotropy in the optical depth can be accounted for by taking the harmonic mean of the opacity,

$$\frac{1}{\bar{\tau}_{\rm eff}} = \frac{1}{A}\int\frac{dA}{\tau(\boldsymbol{r})} \tag{20}$$

(see Appendix D). In practice, the escape of photons is primarily controlled by the minimum optical depth, which is in the polar direction, so in our numerical models we evaluate $\bar{\tau}_{\rm eff}$ with a column density that is 20% of the column in the vertical direction from the point of interest. (3) Finally, we assume that the effect of the velocity field can be approximated by a Doppler line profile of suitable width (see below).

The propagation of resonance line photons in very opaque media has been treated by a number of authors (Adams 1972; Harrington 1973; Hummer & Kunasz 1980; Neufeld 1990). Let the mean optical depth in the line be

$$\bar{\tau} = \frac{1}{\Delta\nu_D}\int\tau_\nu\,d\Delta\nu. \tag{21}$$

In terms of the normalized frequency $x \equiv \Delta\nu/\Delta\nu_D$, we have $\tau_x = \tau_\nu = \bar{\tau}\phi_x$, where ϕ_x is the line profile. In the Doppler core, the line profile is $\phi_x \simeq \exp(-x^2)/\sqrt{\pi}$; in the damping wings it is $\phi_x \simeq a/(\pi x^2)$, where a is the ratio of the natural line width to the Doppler width. In applications, we generally have $a \ll 1$, and in that case the optical depth at line center, τ_0, is related to mean optical depth by $\tau_0 = \bar{\tau}\phi_0 = \bar{\tau}/\sqrt{\pi}$. The opacity is $\kappa_x = \bar{\kappa}\phi_x$, and the mean free path is $\ell_x = 1/\kappa_x$.

As shown by Adams (1972), resonance photons escape in a single longest excursion from line center. After n scatterings, the escaping photon has a frequency shift $x_e \simeq n^{1/2}$ and it has traveled a distance $n^{1/2}\ell_e \simeq n^{1/2}/(\bar{\kappa}\phi_e)$, where $\ell_e = \ell(x_e)$, etc. In order for the photon to escape, this distance must be the size of the region, $L = \bar{\tau}_L/\bar{\kappa}$. This implies $n^{1/2} \simeq \bar{\tau}_L\phi_e$ and $x_e \simeq \bar{\tau}_L\phi_e$, which in turn gives the characteristic frequency of the escaping photons as $x_e \sim (a\bar{\tau}_L)^{1/3}$. The total path length traversed by the escaping photons is about $n^{1/2}L$. As a result, we expect the mean intensity to exceed the incident intensity by a factor of about $n^{1/2} \sim (a\bar{\tau}_L)^{1/3}$.

The velocity field has contributions from thermal motions, turbulent motions, and the overall flow. Thermal and microturbulent velocities are naturally included in Δv_D. In the cases we consider, the overall flow is highly opaque, so it generally does not contribute to the random walk of the photons. If the velocity width of the flow Δv_f (including macroturbulence) is small compared to the line width of the escaping photons, $\Delta v_e \simeq (a\bar{\tau}_{\rm eff})^{1/3}\Delta v_D$ (from Neufeld 1990), then the flow has negligible effect on the escape of the photons. On the other hand, if $\Delta v_f \gg \Delta v_e$, then the effective column density of the gas is reduced. For example, in the simple case in which the velocity varies linearly with

the column density, photons will interact with only a fraction $\Delta v_e/\Delta v_f$ of the gas. If Δv_{e0} is the line width in the absence of any flow velocity, then one can show that the effective column density is reduced by a factor of about $(\Delta v_{e0}/\Delta v_f)^{3/2}$ from the total value. In our numerical models we always set $\Delta v_D = 12.9$ km s^{-1}, the value appropriate for $T = 10^4$ K gas, the assumed temperature of the infalling neutral gas near the protostar. We set Δv_f equal to half the difference in radial velocities of the inner and outer edges of the slab. If $\Delta v_{e0} > \Delta v_f$, which is not usually the case, we reduce the effective column by the factor $(\Delta v_{e0}/\Delta v_f)^{3/2}$.

Appendix B describes the general enhancement in the intensity of photons that are trapped by the Lyα damping wings and, if the columns are very large, by the opacity due to Rayleigh scattering. Thus, photons from the protostellar continuum, outside the frequency interval defined by x_e, can contribute to the radiation pressure. The enhancement in intensity leads to an increase in the radiation pressure so that the momentum transferred from the radiation to the gas is F/c in each optical depth. As shown in Appendix B, the isotropic component of the radiation pressure is

$$P_{\rm rad,\,iso} = \frac{4\pi J_{\rm iso}}{3} = \frac{4\pi}{3}\int d\nu_i \min\left\{ B_{\nu_i}, \frac{8.25 N_{\rm eff,\,20}^{1/3}\Delta v_{D,6}^{-2/3}(F_{\nu_i}/c)}{\min\left(1, 2.62 N_{\rm eff,\,20}^{1/3}\Delta v_{D,6}^{-2/3}\right) + 5.41[\hat{x}_i^2/f(\nu_i)] + \Gamma(\hat{x}_i)} \right\}, \tag{22}$$

where $N_{\rm eff,\,20} \equiv N_{\rm eff}/(10^{20}\ {\rm cm}^{-2})$ and B_{ν_i} is the intensity of a blackbody with a temperature equal to that at the protostellar surface. When this limit is evaluated for the reprocessed Lyα photons, the intensity is limited to that of a blackbody at the temperature of the ionized gas in the H II region (see § B3). This expression is valid provided that $\bar{\tau}_{\rm eff} \gtrsim 1/a$, corresponding to $N_{\rm eff} \gtrsim 10^{16}\Delta v_{D,6}^2$ cm^{-2} for Lyα.

What is the condition for the radiation pressure to halt the accretion? We assume that the accreting gas is inside the sonic point, so that the gas pressure is negligible. For steady, radial flow, the equation of motion of the gas is

$$\rho v\frac{dv}{dr} = -\frac{dP_{\rm rad,\,iso}}{dr} - \frac{\rho G m_*}{r^2}, \tag{23}$$

since we have shown in Appendix C that the radiative force can be represented by the gradient of the isotropic component of the radiation pressure. We assume that the radiation pressure builds up rapidly over a distance small compared to the radius r; this is justified below. Then constancy of the mass flux implies $\rho v \simeq$ const. If the radiative force is to stop the flow in a small distance, then the gravitational force must be negligible in comparison. We then have

$$\frac{d}{dr}\left(\rho v^2 + P_{\rm rad,\,iso}\right) \simeq 0, \tag{24}$$

so that $\rho v^2 + P_{\rm rad,\,iso} \simeq$ const in the deceleration region. When gas enters this region, the radiation pressure is small and $v \simeq v_{\rm ff}$, the free-fall velocity; as the gas decelerates, the radiation pressure rises and v drops. The inflow will be halted if the radiation pressure at the inner edge of the deceleration region is $P_{\rm rad,\,iso} = \rho_{\rm ff} v_{\rm ff}^2$, where $\rho_{\rm ff}$ is the density in the freely falling gas.[4] We have verified this simple argument by solving for the flow in the case that the flux varies as r^{-k_F}, with $k_F > 2$; such a faster than spherical falloff in the flux is expected when the density distribution is not spherically symmetric, so that flux will escape into regions of lower opacity (as in the case of the "flashlight effect"; Yorke & Bodenheimer 1999). We find that the radiation pressure required to halt the infall is within about 10% of $\rho_{\rm ff} v_{\rm ff}^2$ for $k_F > 2.5$. In order to reverse the inflow and eject the matter, the radiation pressure must be twice this, $P_{\rm rad,\,iso} = 2\rho v_{\rm ff}^2$. Of course, a steady radial flow cannot reverse direction. To see that the factor of 2 is required, one can imagine that the flow is inward over half the sky and outward over the other half; to maintain the same accretion rate, the density would have to be twice as large. If the gas is initially in a disk, there is no infall to start with and the pressure required for ejection is $\rho v_{\rm Kep}^2 = \rho v_{\rm ff}^2/2$.

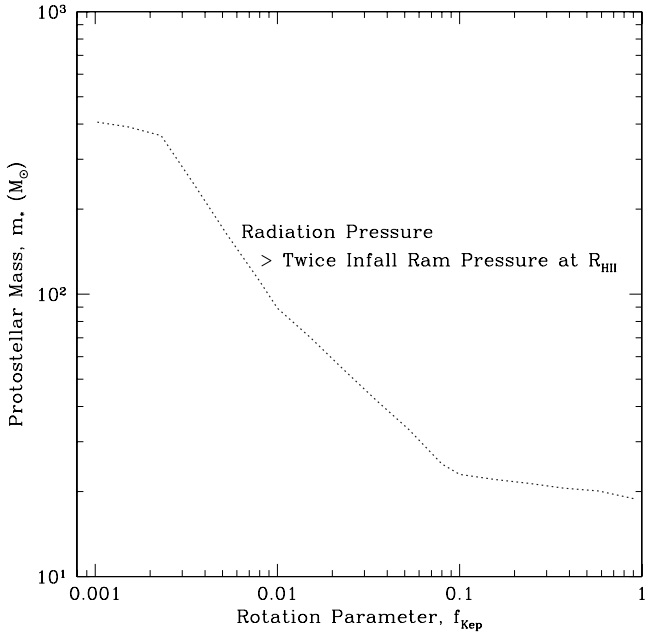

FIG. 3.—Protostellar mass scale at which Lyα radiation pressure becomes twice the ram pressure of the infalling gas at the edge of the H II region along the polar direction as a function of $f_{\rm Kep}$. At this point the radiation pressure is expected to reverse the accretion in the polar direction and evacuate a polar cavity, through which Lyα photons can escape. Thus, this feedback mechanism will act to reduce the efficiency of accretion but will not significantly impede the growth of the star, since most mass is accreted from directions away from the polar axis. [*See the electronic edition of the Journal for a color version of this figure.*]

We evaluate this criterion along the polar axis at the edge of the H II region, which is where the ram pressure of infalling gas is a minimum and where breakout should occur first (Fig. 3). At low values of $f_{\rm Kep}$ the breakout does not occur until the star has reached several hundred solar masses as the photosphere is very large and cool, producing little FUV flux. At reasonable values of $f_{\rm Kep} \gtrsim 0.1$, polar breakout can occur relatively early, at $\sim 20\,M_\odot$. This is the point in the protostellar evolution when the star is starting its rapid contraction to the main sequence, and the surface temperature and luminosity are thus rising. For these values of $f_{\rm Kep}$ the densities and ram pressures become significantly greater as the sight line moves away from the pole. By the time that the radiative flux from the star is large enough to reverse the flow in these directions, a polar cavity would have been blown out, thus reducing the enhancement in the radiation pressure due to trapping of photons. Thus, although Lyα radiation pressure can act to reduce the efficiency of accretion, we expect it to be unable to stop it. Even the reduction of the accretion efficiency is likely to be relatively

[4] Jijina & Adams (1996) have given an alternative criterion based on treating the radiative force per unit mass as the gradient of a potential. Their approach is appropriate when one knows the spatial variation of the force in advance, which is not the case here. One can show that the two approaches are equivalent if the radiative force per unit mass falls off rapidly with r.

modest, since even a small polar cavity can dramatically reduce the radiation pressure in the H II region. In the following sections we consider other feedback mechanisms that are more effective at limiting accretion, although they do so at higher masses. When following the stellar evolution to these masses, we assume that the reduction in accretion efficiency due to Lyα feedback is negligible.

5. IONIZING FEEDBACK AND BREAKOUT OF THE H II REGION

5.1. *Photoionization Heating*

Extreme ultraviolet ($h\nu > 13.6$ eV) radiation from the protostar can ionize infalling neutral gas, creating an H II region. The temperature of the ionized gas is $\sim 2.5 \times 10^4$ K, based on the models of Giroux & Shapiro (1996) and Shapiro et al. (2004) with stellar spectra. The thermal pressure $P \equiv \rho c^2$ of the ionized region is typically much greater than that in neutral gas of the same density because of the elevated temperatures and sound speeds: $c_i = 11.6(T_i/10^4\ \mathrm{K})^{1/2}\ \mathrm{km\ s^{-1}}$. The pressure gradients created at this ionized-neutral boundary can become steep enough to cause the H II region to expand and to dramatically reduce the accretion of gas to the star. In this section we attempt to calculate the point in the protostellar evolution at which this transition occurs. This problem has been considered previously by Omukai & Inutsuka (2002). The new feature in our treatment is that we allow for the rotation of the infalling gas, which can significantly reduce the density near the protostar. As seen below, this completely changes the evolution of the H II region.

As in Paper I, we approximate the density distribution of the infalling gas by the Ulrich (1976) solution. The gas is assumed to be spherically symmetric far from the protostar, and each mass element conserves its angular momentum as it falls ballistically toward the star. Terebey et al. (1984) showed that this solution matches on to an expansion wave solution for the gravitational collapse of a singular isothermal sphere. The resulting density distribution is

$$\rho = \frac{\dot{m}_{*d}\psi(\mu, r)}{4\pi r^{3/2}(2Gm)^{1/2}}, \tag{25}$$

where $\mu = \cos\theta$,

$$\psi(\mu, r) = \left(\frac{2}{1+\mu/\mu_0}\right)^{1/2} \frac{1}{\mu/\mu_0 + 2\mu_0^2(r_d/r)}, \tag{26}$$

and μ_0 is the value of μ far from the protostar. The two angles are related by

$$\frac{r_d}{r} = \frac{\mu_0 - \mu}{\mu_0(1-\mu_0^2)}, \tag{27}$$

which shows that $\mu_0 > \mu$: the gas converges toward the disk plane. Ulrich assumed that the disk had negligible mass, so that $m = m_*$ in equation (25). In our case, m varies smoothly from m_{*d} to m_* as r shrinks from being much greater than r_d to being much less than r_d. This variation in the mass acting on the infalling gas leads to small, unknown deviations from the Ulrich solution. In view of the necessarily approximate nature of the solution and the fact that m_{*d} and m_* differ by only a factor of 4/3 in the fiducial case, we set $m = m_{*d}$ in applying equation (25).

The density factor ψ depends on both the current direction cosine, μ, and the initial one, μ_0, with the two being related by the cubic equation (27). In our analysis, it is convenient to have an approximation for ψ in which the dependence on μ_0 is eliminated:

$$\psi \simeq \left[\frac{2}{1+\max(\mu^{2/3},\, 1-\zeta)}\right]^{1/2} \times \frac{1}{0.5(\zeta - 1 + 3|\zeta - 1|) + 3\mu^{2/3}\min(1,\, \zeta)}, \tag{28}$$

where $\zeta \equiv r_d/r$. This is exact for all r at $\theta = 0$, where $\mu = \mu_0 = 1$, and at $\theta = \pi/2$, in the plane of the disk. It is also exact at $r = r_d$ for all θ. For $r < r_d$ it is accurate to better than 20%; for $r > r_d$, it is accurate to within a factor of 2. To simplify our results, we approximate this further for $r \lesssim 0.5 r_d$ and take

$$\psi \sim \left(\frac{2}{1+\mu}\right)^{1/2} \frac{r}{2r_d} \quad (r \lesssim 0.5 r_d). \tag{29}$$

This approximation is quite accurate at $\mu = \frac{2}{3}$ (better than 20% for $r \le r_d$), but it deteriorates away from there, underestimating the density by a factor of ~ 2 in the plane for $r = \frac{1}{2} r_d$ (the accuracy improves as r decreases). Nonetheless, it suffices to give an analytic estimate for the behavior of the H II region.

5.1.1. *Early Evolution of the* H II *Region*

H II regions are bounded by ionization fronts. Ionization fronts that move faster than about $2c_i$ with respect to the neutral gas, where c_i is the isothermal sound speed of the ionized gas, are termed "R type"; such fronts have little dynamical effect (Spitzer 1978). However, if the velocity of the front slows below $2c_i$, a shock forms in front of the ionization front and the velocity of the front into the shocked gas falls to $\simeq c_n^2/2c_i$, where $c_n \ll c_i$ is the isothermal sound speed of the shocked neutral gas; such ionization fronts are termed "D type." When the H II region first forms, it is embedded in gas falling inward with a velocity $v_{\rm ff} \gg 2c_i$. As a result, the ionization front is initially R type, and the radius of the H II region, $r_{\rm H\,II}$, is determined by ionization balance.

Since the density of the infalling gas depends on the angle θ relative to the axis of rotation, $r_{\rm H\,II}$ depends on angle also. We determine this radius in the sector approximation, in which ionizations balance recombinations in each element of solid angle:

$$\frac{dS}{d\Omega} = \frac{S}{4\pi} = \int_{r_*}^{r_{\rm H\,II}} r^2 \alpha^{(2)} n_e n_p\, dr, \tag{30}$$

where S is the rate of emission of ionizing photons and $\alpha^{(2)} \simeq 2.6 \times 10^{-13} T_4^{-0.8}\ \mathrm{cm^3\ s^{-1}}$ is the recombination rate to the excited states of ionized hydrogen. In writing equation (30), we have made three approximations. First, we have assumed that the rate of emission of ionizing photons is much greater than the rate of accretion of hydrogen atoms so that ionizations and recombinations are very nearly in balance (note that advection of neutral H into the H II region is allowed for in the numerical models). For a mass accretion rate of $10^{-3}\ M_\odot\ \mathrm{yr^{-1}}$ the hydrogen accretion rate is about $3 \times 10^{46}\ \mathrm{s^{-1}}$. The mass at which the ionizing photon luminosity exceeds this value depends on $f_{\rm Kep}$; for the fiducial case of $f_{\rm Kep} = 0.5$, this occurs at about $m_* \simeq 20\ M_\odot$. Second, we have assumed that in the outer parts of the H II region, where the helium is singly ionized for stellar temperatures $\sim 10^5$ K, each recombination of He^+ results in one H ionization, whereas it actually results in about $\frac{2}{3}$ of an ionization at the relevant densities ($>10^4\ \mathrm{cm^{-3}}$; Osterbrock 1989, pp. 23–29). In fact, the abundance of He is sufficiently small (~ 0.08) that we henceforth neglect it in our analytic estimates (however, we do not neglect its contribution to

the mass density, nor is it neglected in the numerical calculations). Finally, we have ignored photoionization from the $n = 2$ level of H, so that our calculation somewhat underestimates the size of the ionized region, although this is not very important at the densities resulting from realistic values of $f_{\rm Kep}$.

With the density distribution given by equation (25), equation (30) becomes

$$S = \frac{\alpha^{(2)} \dot{m}_{*d}^2 I}{8\pi \mu_{\rm H}^2 G m_{*d}} \equiv S_{\rm cr} I, \tag{31}$$

where $\mu_{\rm H} = 2.20 \times 10^{-24}$ g is the mass per hydrogen and

$$I \equiv \int_{r_*}^{r_{\rm H\,II}} \frac{\psi^2(\mu, r)}{r}\, dr. \tag{32}$$

We have set $m = m_{*d}$ in equation (25) in accord with the discussion following equation (27). Equation (31) reduces to that of Omukai & Inutsuka (2002) for $\psi = \ln(r_{\rm H\,II}/r_*)$ (and if $\mu_{\rm H}$ is replaced by m_p, $\dot{m}_{*d}$ by $\dot{m}_*$, and m_{*d} by m_*). As shown by Omukai & Inutsuka (2002), an H II region in an $r^{-3/2}$ density profile is confined to the vicinity of the star for $S \lesssim S_{\rm cr}$ and expands to exponentially large distances as S increases above $S_{\rm cr}$. Numerically, we have

$$S_{\rm cr} = 3.07 \times 10^{50} \left(\frac{2.5}{T_4}\right)^{0.8} \frac{\dot{m}_{*d,-3}^2}{m_{*d,2}} \text{ photons s}^{-1}$$
$$\rightarrow 2.36 \times 10^{51} \left(\frac{2.5}{T_4}\right)^{0.8} \frac{K'^{30/7}}{m_{*,2}^{13/7}} \text{ photons s}^{-1}. \tag{33}$$

By comparison, the ionizing luminosity of a Population III star is

$$S \simeq 7.9 \times 10^{49} \phi_S m_{*,2}^{1.5} \text{ photons s}^{-1}, \tag{34}$$

which for $\phi_S = 1$ is a fit to Schaerer's (2002) results for the ionizing luminosity of main-sequence primordial stars; the fit is accurate to within about 5% for $60\ M_\odot \lesssim m_* \lesssim 300\ M_\odot$. As shown in Paper I, the ionizing luminosity can be less than the main-sequence value ($\phi_S < 1$) when the star is still contracting toward the main sequence, and it can be greater when it is accreting while on the main sequence; for the case illustrated in Paper I, $\phi_S \lesssim 2$. If the accretion rate is not reduced by feedback effects, S would not exceed $S_{\rm cr}$ until $m_* > 275 K'^{14/47}\ M_\odot$ for $T_4 = 2.5$. However, as seen below, rotation makes the factor I small and allows the H II region to expand until it is almost as large as the disk even when the mass is less than this.

At early times we have $r_{\rm H\,II} \ll r_d$ so that we can use the approximation given by equation (29) for the density. As a result, we find

$$\frac{S}{S_{\rm cr}} = I \simeq \frac{1}{4(1+\mu)} \left(\frac{r_{\rm H\,II}}{r_d}\right)^2. \tag{35}$$

With equations (33) and (34), we then obtain

$$\frac{r_{\rm H\,II}}{r_d} = 1.01(1+\mu)^{1/2}(1+f_d)^{1/2} \phi_S^{1/2} \left(\frac{T_4}{2.5}\right)^{0.4} \frac{m_{*,2}^{1.25}}{\dot{m}_{*d,-3}} \tag{36}$$

$$\rightarrow 0.37(1+\mu)^{1/2} \phi_S^{1/2} \left(\frac{T_4}{2.5}\right)^{0.4} \frac{m_{*,2}^{47/28}}{K'^{15/7}}. \tag{37}$$

Recall that "$\rightarrow$" indicates that we have taken $m_{*d} = (4/3)m_*$. We see that for $m_{*,2} \lesssim 1$ we have $r_{\rm H\,II} \lesssim 0.5 r_d$, so that our approximation for the density, equation (29), is reasonably accurate at early times. The radius of the H II region is then

$$r_{\rm H\,II} = 5.40 \times 10^{15} (1+\mu)^{1/2} \phi_S^{1/2} \left(\frac{T_4}{2.5}\right)^{0.4} \left(\frac{f_{\rm Kep}}{0.5}\right)^2$$
$$\times \frac{(1+f_d)^{31/14} m_{*,2}^3}{K'^{25/7}} \text{ cm} \quad (m_{*,2} \lesssim 1), \tag{38}$$

where we have set the star formation efficiencies ϵ_{*d} and $\bar{\epsilon}_{*d}$ equal to unity and where we have made the approximation $83/28 \simeq 3$ in the exponent of $m_{*,2}$. As the stellar mass increases above $100\ M_\odot$, the approximation for the density, equation (29), increasingly overestimates the density except near the equator; as a result, the radius of the H II region, $r_{\rm H\,II}$, becomes larger than the value given in equation (38) except near the plane of the disk, where the high density traps the H II region. As remarked above, for $S > S_{\rm cr}$, which occurs for $m_{*,2} > 2.75$, if the accretion continues unabated by feedback, $r_{\rm H\,II}$ increases exponentially with S (Omukai & Inutsuka 2002).

5.1.2. *Later Evolution of the* H II *Region: Suppression of Accretion*

According to equation (38), the radius of the H II region expands on the protostellar evolution timescale $\sim 10^4$ yr, which is far longer than the dynamical time $r_{\rm H\,II}/2c_i \sim 10^2$ yr. As a result, the velocity of the ionization front relative to the infalling gas is very nearly equal to the free-fall velocity. The first phase of evolution of the H II region ends when it expands to the point that the radius becomes comparable to the gravitational radius,

$$r_g \equiv \frac{G\phi_{\rm Edd} m_{*d}}{c_i^2} = 3.92 \times 10^{15} \phi_{\rm Edd} \left(\frac{2.5}{T_4}\right) m_{*d,2} \text{ cm}, \tag{39}$$

where we have taken the gravitating mass to be m_{*d}. Here we have allowed for the decrease in the radiation pressure due to electron scattering through the factor

$$\phi_{\rm Edd} \equiv 1 - \frac{L}{L_{\rm Edd}}, \tag{40}$$

where $L_{\rm Edd} = 4\pi G m c/\kappa_{\rm T}$ is the Eddington limit. In Paper I we found that $L/L_{\rm Edd} \sim 0.6$–0.8 for $m = m_* \sim 10^2\ M_\odot$, which corresponds to $\phi_{\rm Edd} \simeq 0.2$–$0.4$. Equations (38) and (39) relate the protostellar mass to $r_{\rm H\,II}/r_g$,

$$m_{*,2} = 0.85 \left[\frac{\phi_{\rm Edd}^{1/2} K'^{25/14}}{(1+\mu)^{1/4}(1+f_d)^{17/28}\phi_S^{1/4}}\right]$$
$$\times \left(\frac{2.5}{T_4}\right)^{0.7} \left(\frac{0.5}{f_{\rm Kep}}\right) \left(\frac{r_{\rm H\,II}}{r_g}\right)^{1/2}. \tag{41}$$

Keep in mind that this relation is valid only for $m_{*,2} \lesssim 1$, so that $f_{\rm Kep}$ cannot be small. This condition is satisfied insofar as the simulations of ABN02 are representative of the angular momentum of the accreting gas, since they give $f_{\rm Kep} \sim 0.5$.

When the H II region expands to the point that $v_{\rm ff} = 2c_i$, a shock front forms and the ionization front becomes D type; this occurs at $r_{\rm H\,II} = r_g/2$. The accretion rate through the H II region will begin to decrease at this point. Since the shocked neutral gas is denser than the ionized gas in the H II region, the accelerating expansion of the shocked shell is subject to the Rayleigh-Taylor instability, and as a result it is difficult to estimate by how much

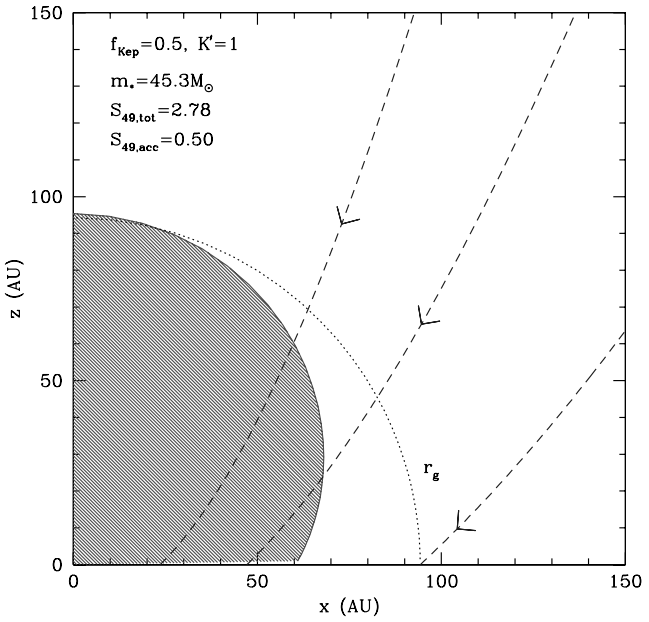

FIG. 4.—Geometry of the H II region (*shaded*) assuming the sector approximation (see text) during the breakout phase for the fiducial model with $K' = 1$ and $f_{\rm Kep} = 0.5$. The protostar is at (0, 0) and the disk is in the $z = 0$ plane. At this stage, the star has $m_* = 45\ M_\odot$ and a total ionizing photon luminosity of $S_{49,\,\rm tot} = 2.78$, of which $S_{49,\,\rm acc} = 0.50$ comes from accretion. The H II region has just recently expanded beyond r_g (at 94 AU) in the polar direction. The geometry of several accretion streamlines is shown by the dashed lines. [*See the electronic edition of the Journal for a color version of this figure.*]

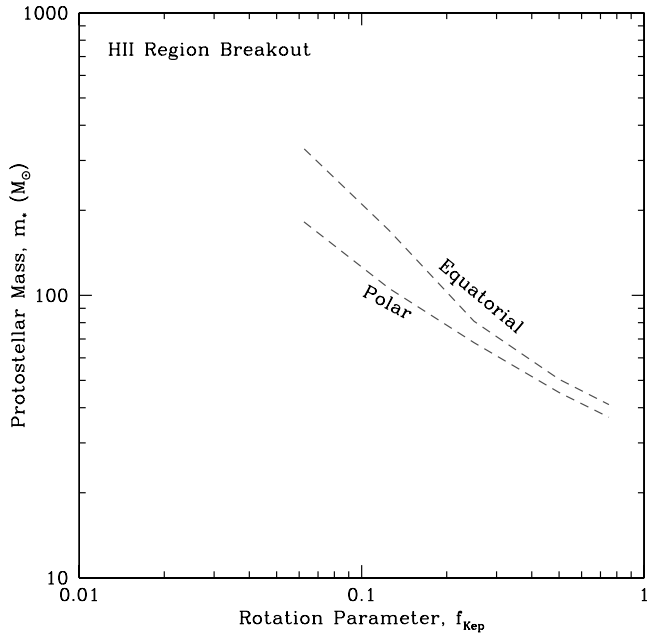

FIG. 5.—Mass scales of H II region breakout as a function of the rotation parameter $f_{\rm Kep}$. The lower dashed line marked "Polar" shows the mass scale of the protostar at which the H II region reaches r_g (based on star plus disk mass) along the rotation axis of the protostar. The upper dashed line marked "Equatorial" shows the mass scale of the protostar when the H II region reaches r_g in a direction just above the disk plane ($0.9\pi/2$ from the rotation axis). Note that this condition for equatorial H II region breakout ignores the effects of reduced accretion rates from prior polar H II region breakout, although such effects are accounted for in the full feedback+evolution models presented below. [*See the electronic edition of the Journal for a color version of this figure.*]

the accretion is reduced. While the shell is moving slowly, it can fall onto the disk and accrete that way. However, once the shocked shell is moving faster than the local free-fall velocity, it seems unlikely that any significant further accretion can occur. To obtain an approximate upper limit on the accretion through the H II region, we assume that, from a given direction, the accretion is unimpeded until the H II region has expanded to a radius equal to r_g. Because of the declining density distribution in the infall envelope, the H II region is expanding relatively rapidly at this stage and so soon ionizes a large region beyond r_g, which we expect leads to a substantial reduction in accretion rate from the affected directions. This approximation needs to be checked with multidimensional radiation hydrodynamical simulations. It is important to bear in mind that this suppression of the accretion occurs only in the ionized gas. Gas in the shadow of the accretion disk around the star can continue to accrete, as discussed below.

In Figure 4 we show the geometry of the H II region near the point of polar breakout of the ionized gas beyond r_g. In this calculation the protostellar evolution has been followed as described in Paper I, but now including the effects of a reduction in accretion rate once the H II region breaks out beyond r_g. This has only just started to occur at the point of the evolution shown in the figure. We have assumed that there is negligible reduction in the accretion rate because of the Lyα radiation feedback since we expect its effects to be limited to relatively small angles around the polar axis. The extent of the H II region is calculated using the sector approximation using the density distribution model of Ulrich (1976) as described above. We include the effect of electron scattering, but not force due to photoionization, which is discussed below. The effect of radiation pressure due to photoionization is strongest for purely radial infall, so its neglect is not critical for the models presented here. We do allow for advection of neutrals into the H II region, although they are not very important by the time the protostar is $\sim 100\ M_\odot$. A temperature of 2.5×10^4 K was adopted for the ionized gas, which affects the value of r_g. Note that in Figure 4 we have assumed an infinitely thin accretion disk. The polar and equatorial breakout conditions are shown as a function of $f_{\rm Kep}$ in Figure 5. Once the protostar has reached the masses indicated by the "Equatorial" line in this figure, we do not expect accretion to be able to proceed from directions that have a direct line of sight to the protostar, i.e., those directions that are not shielded by the accretion disk. Thus, in most cases we do not expect H II region breakout to set the final mass of the star, but rather to cause a decrease in accretion efficiency that starts to become important at about $50\ M_\odot$ in the fiducial case. The actual reduction in accretion efficiency depends on the thickness of the accretion disk, to be discussed below (§ 6).

We can compare the analytic prediction for H II region breakout (eq. [41]) with our numerical calculation, which for the fiducial model ($f_{\rm Kep} = 0.5, K' = 1, T_4 = 2.5, f_d = \frac{1}{3}$) finds breakout in the polar direction at a mass of $45.3\ M_\odot$. At this point the total H-ionizing luminosity is $S_{49} = 2.78$ so that $\phi_S = 1.15$ and the bolometric luminosity is $5.95 \times 10^5\ L_\odot$ so that $\phi_{\rm Edd} = 0.59$. With these values, the analytic estimate for the mass at which polar ($\mu = 1$) H II region breakout ($r_{\rm H\,II} = r_g$) occurs (eq. [41]) is $44.7\ M_\odot$, in excellent agreement with the numerical value. In Figure 5 we see that the mass at which the H II region breaks out does not scale as a simple power of $f_{\rm Kep}$. This is because $\phi_{\rm Edd}$ and ϕ_S vary with stellar mass, especially for $m_* \lesssim 100\ M_\odot$.

5.2. *Radiation Pressure due to Photoionization*

Continuum radiation is dynamically coupled to the gas in the H II region, both through Thomson scattering and through photoionization. Since the H II region is optically thin to Thomson scattering, it effectively reduces the force of gravity by a factor $\phi_{\rm Edd} = 1 - L/L_{\rm Edd}$, which as discussed above is $\sim$0.2–0.4 for

$m_{*,2} \sim 1$. At distances large enough that the mass acting on the gas is m_{*d}, $L/L_{\rm Edd}$ is reduced by a factor $1 + f_d$. Keep in mind that the decrease in the effective gravity due to electron scattering reduces the accretion rate of ionized gas only; it does not affect the accretion of neutral gas outside the H II region onto the disk.

Every photoionization results in a transfer of momentum $h\nu_i/c$ to the gas, where $h\nu_i$ is the mean energy of the photons that ionize the gas. The importance of radiation pressure associated with photoionization has long been appreciated in studies of active galactic nuclei (AGNs) and X-ray sources (e.g., Tarter & McKee 1973); Haehnelt (1995) pointed out its importance in the formation of the first galaxies, and Omukai & Inutsuka (2002) discussed its role in the formation of the first stars. They showed that, under the assumption of perfect spherical symmetry, radiation pressure would have the counterintuitive effect of *reducing* the size of the H II region, thereby eliminating any feedback effect on the growth of the protostar. Since photoionizations are balanced by recombinations, the radiative force is given by $\alpha^{(2)} n_p^2 (h\nu_i/c)$. Generalizing their treatment to include electron scattering, we find that this radiative force balances the effective gravity at a critical density $n_{\rm cr}$ given by

$$\alpha^{(2)} n_{\rm cr}^2 \left(\frac{h\nu_i}{c}\right) = \frac{\phi_{\rm Edd}\rho_{\rm cr} G m_{*d}}{r^2}, \tag{42}$$

so that

$$n_{\rm cr} = 2.15\times10^6 \phi_{\rm Edd}\left(\frac{T_4}{2.5}\right)^{0.8} \frac{m_{*d,2}}{r_{16}^2}\ {\rm cm}^{-3}, \tag{43}$$

where we have assumed a typical ionizing photon energy of 1.5×13.6 eV. For gas accreting in free fall (i.e., it enters the H II region at a velocity that is unaffected by radiation pressure), this corresponds to a critical radius

$$r_{\rm cr} = 2.36\times10^{14} \phi_{\rm Edd}^2 \left(\frac{T_4}{2.5}\right)^{1.6} \frac{m_{*d,2}^3}{\dot m_{*d,-3}^2}\ {\rm cm} \tag{44}$$

$$\rightarrow 5.49\times10^{13} \phi_{\rm Edd}^2 \left(\frac{T_4}{2.5}\right)^{1.6} \frac{m_{*,2}^{27/7}}{K'^{30/7}}\ {\rm cm}. \tag{45}$$

Even for $\phi_{\rm Edd} = 1$, this radius is typically a few AU in size, and the infall velocity is highly supersonic relative to the sound speed of the ionized gas. Omukai & Inutsuka (2002) showed that as the ionizing flux from the protostar increased, the radius of the H II region would increase until it approached $r_{\rm cr}$. As it did so, the inflow velocity would drop, the density would rise, and the accreting gas would be able to absorb a larger number of ionizing photons. In fact, the accretion flow inside $r_{\rm cr}$ could absorb more ionizing photons than any star could emit. As a result, the H II region would remain trapped at small radii and the gas would continue to accrete supersonically onto the star. It is not clear that this flow would be stable in three dimensions, however, since a fluctuation that placed an element of ionized gas at $r > r_{\rm cr}$ would result in a net outward force on the gas.

Angular momentum in the accreting gas changes this picture completely: the density of the infalling gas is reduced inside the disk radius r_d (eq. [16]), which is generally much larger than $r_{\rm cr}$:

$$\frac{r_d}{r_{\rm cr}} = 509 \left(\frac{K'^{20/7}}{\phi_{\rm Edd}^2}\right)\left(\frac{T_4}{2.5}\right)^{-1.6}\left(\frac{f_{\rm Kep}}{0.5}\right)^2 m_{*,2}^{-18/7}. \tag{46}$$

For typical masses $m_* \sim 10^2\ M_\odot$, the disk radius is larger than $r_{\rm cr}$ only for very low rotation, $f_{\rm Kep} \lesssim 0.02\phi_{\rm Edd}$. Repeating the analysis that led to equation (45) with the density appropriate for rotating infall (eqs. [25] and [29]), we find

$$r_{\rm cr} \simeq 2^{2/3}\left(\frac{1+\mu}{2}\right)^{1/3} r_{\rm cr,\,spherical}^{1/3} r_d^{2/3} \tag{47}$$

$$\simeq 5.5\times10^{15}\phi_{\rm Edd}^{2/3}\left(\frac{1+\mu}{2}\right)^{1/3}\left(\frac{f_{\rm Kep}}{0.5}\right)^{4/3} \times \left(\frac{T_4}{2.5}\right)^{0.53} \frac{m_{*,2}^{15/7}}{K'^{50/21}}\ {\rm cm}, \tag{48}$$

where $r_{\rm cr,\,spherical}$ is the critical radius for spherical infall (eq. [45]). This result shows that in a rotating infall, the critical radius beyond which radiation pressure dominates the effective gravity is intermediate between the critical radius in the spherical case and the disk radius. Comparison with equation (39) shows that in the rotating case, the critical radius is comparable to the gravitational radius, where pressure effects can drive the outward expansion of the H II region. It therefore appears that for typical values of the rotation, radiation pressure due to photoionization cannot result in the confinement of the H II region; correspondingly, feedback by the H II region cannot be curtailed by this effect.

6. DISK SHADOWING

An optically thick accretion disk is able to shield part of the outer accretion flow from direct protostellar feedback. In order to determine how effective this shielding is, we must know the thickness of the accretion disk. With a few significant exceptions (e.g., Paczyński & Bisnovati-Kogan 1981; Meyer & Meyer-Hofmeister 1982; D'Alessio et al. 1998), almost all the work on accretion disks has gone into determining their radial structure; the vertical structure is generally integrated over. Here we estimate the thickness of the disk under the assumption that it is geometrically thin but very optically thick. We neglect convective and turbulent transport in the disk, which D'Alessio et al. (1998) found to be small for the cases they considered. We focus on the inner parts of the disk, where self-gravity is unimportant (Tan & Blackman 2004). For simplicity, we neglect heating of the disk by irradiation from the central source; our estimate of the disk thickness is thus a lower limit to the true thickness.

The radial structure of the disk is governed by the equations of energy conservation and of angular momentum conservation. Energy conservation gives the emergent flux as (Paper I)

$$F_0 = \frac{\dot m_*}{4\pi\varpi}\frac{\partial}{\partial\varpi}\left(\frac{5}{3}\bar\epsilon_{\rm th} + \bar\epsilon_I\right) + \frac{3Gm_*\dot m_* f}{8\pi\varpi^3} \tag{49}$$

$$\equiv \phi_I\left(\frac{3Gm_*\dot m_* f}{8\pi\varpi^3}\right). \tag{50}$$

Here

$$f \equiv 1 - \left(\frac{\varpi_0}{\varpi}\right)^{1/2} \tag{51}$$

is the factor that embodies the boundary condition that angular momentum cannot be transferred across a surface on which the angular velocity has no gradient; ϖ_0 is the cylindrical radius at which $\partial\Omega/\partial\varpi$ vanishes, which we take to be equal to the stellar radius. The dimensionless factor ϕ_I describes the advection of thermal and internal energy in the disk and is generally less than unity.

To evaluate the angular momentum transfer in the disk, we adopt the α-disk model of Shakura & Sunyaev (1973), in which

the transverse stress in the disk is proportional to the pressure, $w_{\varpi\phi} = -(3/2)\alpha P$ (we have included the factor 3/2 to conform with convention; Frank et al. 1995). The equation describing angular momentum transport is then

$$\dot{m}_* \Omega f = 6\pi\alpha \int_0^{z_s} P\, dz, \tag{52}$$

where z_s is the height of the surface of the disk.

The vertical structure of the disk is governed by three equations. First is the first moment of the radiative transfer equation,

$$\frac{\partial P_{\rm rad}}{\partial z} = -\frac{\rho \kappa_F F}{c}, \tag{53}$$

where κ_F is the flux-weighted mean opacity per unit mass and $F(z)$ is the radiative flux. We assume that the effective optical depth for true absorption, $\tau^* = (\tau_{\rm abs}\tau_{\rm scatt})^{1/2}$, is much greater than unity so that the gas is approximately in LTE (Shakura & Sunyaev 1973; Artemova et al. 1996). Then $P_{\rm rad} \simeq \frac{1}{3} a T^4$ and $\kappa_F \simeq \kappa_{\rm R}$, where $\kappa_{\rm R}$ is the Rosseland mean opacity per unit mass, so that equation (53) reduces to the equation of radiative diffusion,

$$\frac{\partial T}{\partial z} = -\frac{3\kappa_{\rm R}\rho F}{16\sigma T^3}. \tag{54}$$

The second equation describes the growth of the flux due to viscous dissipation,

$$\frac{\partial F}{\partial z} = -\phi_I w_{\varpi\phi}\varpi \frac{\partial \Omega}{\partial \varpi} = \frac{9}{4}\phi_I \alpha \Omega P \tag{55}$$

(Shu 1992). We have included the factor ϕ_I to allow for the reduction in the flux by the advection of internal energy. In addition to the factor $(3/2)\phi_I$, equation (55) differs from the expression adopted by Shakura & Sunyaev (1973) in that it has $\partial F/\partial z \propto P$ rather than $\propto \rho$. One can show, however, that the height of the disk is very insensitive to this change. Integration of equation (55) together with equation (52) leads directly to the energy equation (50).

Finally, we have the equation of hydrostatic equilibrium,

$$\frac{\partial P}{\partial z} = -\frac{\rho G m_* z}{\varpi^3}, \tag{56}$$

where the pressure P includes both gas pressure and radiation pressure,

$$P = P_g + P_{\rm rad} = \frac{\rho k T}{\mu} + \frac{4\sigma T^4}{3c}. \tag{57}$$

For a primordial gas with a helium fraction of 0.079, the mean mass per particle is

$$\mu \simeq \frac{1.32 m_{\rm H}}{1.08 + x_e} = \frac{2.20\times 10^{-24}}{1.08 + x_e}\ {\rm g}, \tag{58}$$

where $x_e \equiv n_e/n_{\rm H}$ is the ionization fraction relative to hydrogen; for a fully ionized primordial gas, $\mu = 0.98\times 10^{-24}$ g. With the aid of equation (54), the equation of hydrostatic equilibrium becomes

$$\frac{\partial \rho}{\partial z} = \left(\frac{kT}{\mu}\right)^{-1}\left[-\frac{G m_* \rho z}{\varpi^3} + \frac{\rho\kappa_{\rm R} F}{c}\left(1 + \frac{3kc\rho}{16\mu\sigma T^3}\right)\right]. \tag{59}$$

This is a two-point boundary value problem, in which $F = F_0$ at the surface of the disk and $F = 0$ at the midplane. We assume that the disk is very opaque, so that we can neglect the flux generated above the photosphere; we can therefore apply the surface boundary conditions at the photosphere, located at $z_{\rm ph}$. Since we have assumed that the disk is opaque and are neglecting irradiation, the surface temperature is small compared to the central temperature; as a result, the scale height near the surface is small and $z_{\rm ph} \simeq z_s$. The temperature at the photosphere is the effective temperature, which is related to the emergent flux by $F_0 = \sigma T_{\rm eff}^4$.

We have addressed this problem both analytically and numerically. The case of pure radiation pressure is trivial to treat analytically, since hydrostatic equilibrium gives

$$\frac{\kappa_{\rm R} F}{c} = \frac{G m_* z}{\varpi^3}, \tag{60}$$

which is true throughout the disk. At the surface of the disk (which is denoted z_{sr} for a radiation-pressure supported disk) this gives

$$z_{sr} = \frac{\kappa_{{\rm R},s} F_0 \varpi^3}{G m_* c}, \tag{61}$$

where $\kappa_{{\rm R},s}$ is the opacity at the disk surface. With the aid of equation (50), this becomes

$$z_{sr} = \left(\frac{3\phi_I \kappa_{{\rm R},s}}{8\pi c}\right)\dot{m}_* f \tag{62}$$

$$= 8.77\times 10^{10}\left(\frac{\kappa_{{\rm R},s}}{\kappa_{\rm T}}\right)\phi_I \dot{m}_{*,-3} f\ {\rm cm}, \tag{63}$$

where we assume that $\dot{m}_* = \dot{m}_{*d}/(1+f_d) \rightarrow \frac{3}{4}\dot{m}_{*d}$ and where $\kappa_{\rm T} = (n_e/\rho)\sigma_{\rm T} = 0.35$ g cm^{-2} is the opacity due to electron scattering for fully ionized primordial gas. Note that the thickness of a radiation-supported disk depends only weakly on radius through the factor $f = 1 - (\varpi_0/\varpi)^{1/2}$ and possibly through a variation in the opacity at the surface.

The case of a disk supported by gas pressure is more complicated and is discussed in Appendix E for the case of constant opacity. There we show that the height of such a disk is

$$z_{sg} \simeq 1.21\times 10^{10}\left(\frac{\phi_I \bar{\kappa}_{\rm R}}{\alpha_{-2}\kappa_{\rm T}}\right)^{1/10}\left(\frac{\varpi}{R_\odot}\right)^{21/20}\frac{\left(\dot{m}_{*,-3} f\right)^{1/5}}{m_{*,2}^{7/20}}\ {\rm cm}, \tag{64}$$

where we have normalized α to a typical value of 0.01. In the above expression, we have replaced the constant opacity in the derivation in Appendix E with a suitable mean value. Observe that the height of a disk supported by gas pressure scales almost linearly with ϖ, so that the aspect ratio is approximately constant.

Numerical solution of the structure equations shows that when both radiation pressure and gas pressure are important, the approximation

$$z_s \simeq \left(z_{sr}^{5/4} + z_{sg}^{5/4}\right)^{4/5} \tag{65}$$

is accurate to better than 10% over the range $10^{-4} \lesssim \alpha \lesssim 10^{-2}$, $\kappa_{\rm R} \simeq \kappa_{\rm T}$, $10^4\ {\rm K} \lesssim T_{\rm eff} \lesssim 10^6$ K, and $0.01 \lesssim z_{sr}/z_{sg} \lesssim 10$, provided that the opacity is constant.

We have also solved the equations for the vertical structure of the disk numerically with a realistic opacity variation with density

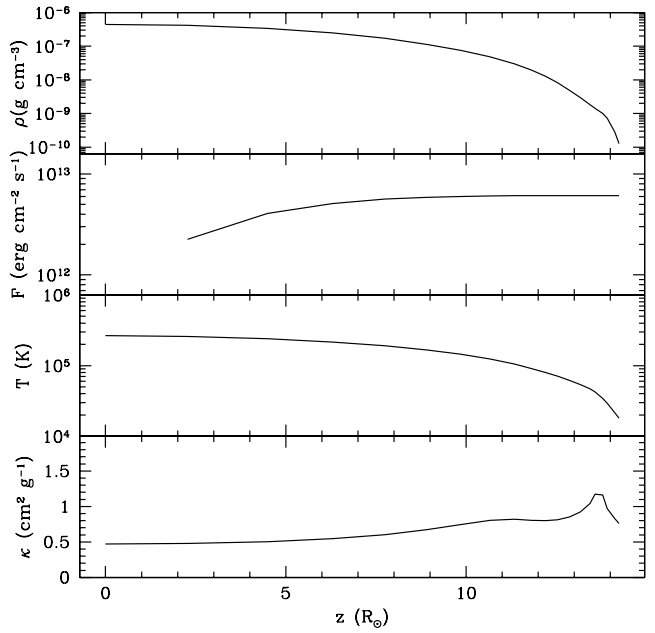

FIG. 6.—Vertical structure of the accretion disk at $r = 10r_* \simeq 43\,R_\odot$ for $m_* = 100\,M_\odot$, $K' = 1$, $f_{\rm Kep} = 0.5$, and no reduction in accretion efficiency due to feedback.

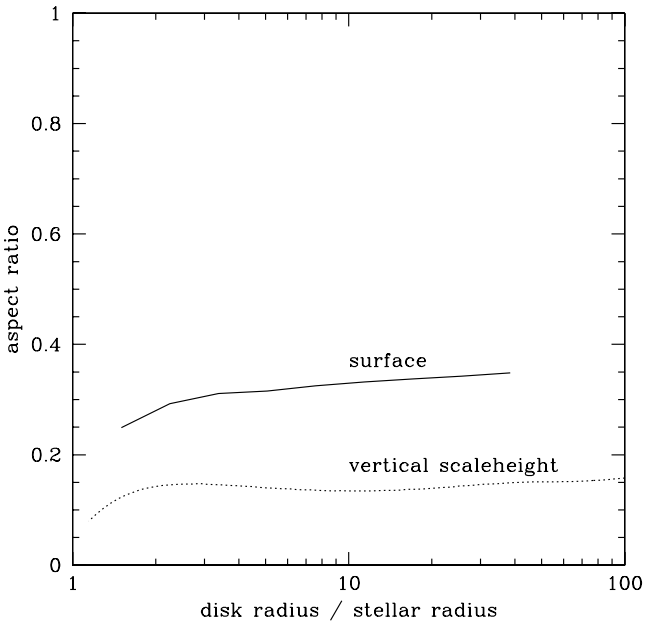

FIG. 7.—Radial dependence of the aspect ratio of the disk surface, z_s/ϖ, and disk density vertical scale height, h/ϖ, for $m_* = 100\,M_\odot$, $K' = 1$, $f_{\rm Kep} = 0.5$, and no reduction in accretion efficiency due to feedback.

and temperature (Iglesias & Rogers 1996). We follow the disk structure during the course of the protostellar evolution (i.e., as m_*, $\dot{m}_*$, and r_* evolve). We adopt an α-viscosity parameter of 0.01, typical of values associated with the magnetorotational instability (Balbus & Hawley 1998; Tan & Blackman 2004), although the disk thickness is not very sensitive to this choice. An example of the vertical disk structure is shown in Figure 6 for a location at $10R_*$ around a $100\,M_\odot$ main-sequence star, accreting at $2.4 \times 10^{-3}\,M_\odot\ {\rm yr}^{-1}$, i.e., the fiducial rate from a $K' = 1$ core with no reduction due to feedback. The numerical value of z_s/ϖ is 0.33. This compares with an analytic estimate based on equation (65) of 0.31, where we adopted $\kappa_{{\rm R},s} = 0.75\ {\rm cm}^2\ {\rm g}^{-1}$ and $\bar{\kappa}_{\rm R} = 0.6\ {\rm cm}^2\ {\rm g}^{-1}$ (Fig. 6).

The radial variation in the density scale height and disk surface height for the above model is shown in Figure 7. Note that z_s/ϖ is approximately constant with ϖ. For simplicity, in our numerical models we evaluate z_s/ϖ at a radial location $\varpi = 10R_*$ and use this to evaluate the fraction of the sky shielded by the disk. In the example shown in Figures 6 and 7, $z_s/\varpi = 0.33$ at this location, and the fraction of the sky shadowed by this disk photosphere is $f_{\rm sh} = 0.31$. If the matter at infinity were spherically distributed in the envelope, then this would be the approximate accretion efficiency once the H II region had expanded to large distances (and assuming that all material in the shadow of the disk remained neutral). Note that the disk model in the numerical example given above is somewhat thicker than would be present around a $100\,M_\odot$ star accreting from a $K' = 1$ core, since the accretion rate would have been reduced by feedback. Our numerical models of the growth of the protostar account for such effects self-consistently.

7. DISK PHOTOEVAPORATION

As we have seen, in the presence of rotation the various feedback mechanisms discussed above will first disrupt infall in the polar direction and may leave behind much of the material in the equatorial plane. Material close to the plane will be shielded from the feedback effects by the formation of an accretion disk. However, this gas is subject to disk photoevaporation, and accretion will cease when the photoevaporation rate exceeds the accretion rate onto the star-disk system.

To estimate when this criterion is reached, we apply the model of Hollenbach et al. (1994) to estimate the rate of photoevaporation from the disk. This rate is calculated assuming a steady disk with no infall from above or below. The diffuse ionizing flux, reprocessed through the flared atmosphere of the disk, illuminates and ionizes material near and beyond r_g. Hollenbach et al. (1994) considered the possibility that the disk would be flattened due to a stellar wind, but we use the results of their weak wind case. The photoevaporation rate is calculated via

$$\dot{m}_{\rm evap} = 2\mu_{\rm H} v \int_{r_g}^{\infty} 2\pi n_0(r) r\, dr, \tag{66}$$

where the flow velocity, v, is set equal to the ionized gas sound speed, $c_i = 18.4(T_4/2.5)^{1/2}$ km s^{-1}, and n_0 is the density of ionized gas at the base of the ionized disk atmosphere. Their analysis gives

$$\dot{m}_{\rm evap} = 4.1 \times 10^{-5} S_{49}^{1/2} T_4^{0.4} m_{*d,2}^{1/2}\ M_\odot\ {\rm yr}^{-1}. \tag{67}$$

As they acknowledge, this result is quite approximate, and a numerical study of this problem would be worthwhile. For primordial stars with an ionizing luminosity given by equation (34), the photoevaporation rate becomes

$$\dot{m}_{\rm evap} = 1.70 \times 10^{-4} \phi_S^{1/2} (1+f_d)^{1/2} \left(\frac{T_4}{2.5}\right)^{0.4} m_{*,2}^{5/4}\ M_\odot\ {\rm yr}^{-1}. \tag{68}$$

There are two corrections that could be applied to this result. First, Begelman et al. (1983) and Woods et al. (1996) showed that for analogous winds from AGN disks, the flow can start from radii well inside r_g. Numerically integrating the expression given by Woods et al. (1996), we find that mass loss inside r_g increases

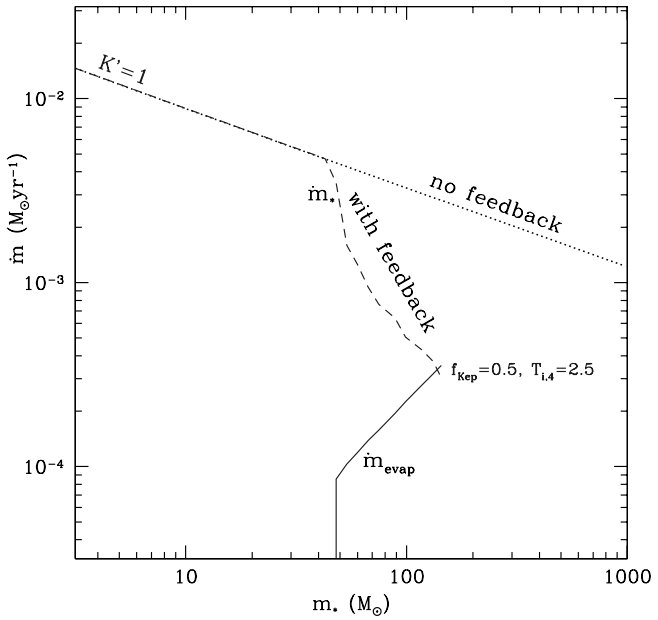

FIG. 8.—Feedback-limited accretion: fiducial case. The evolution of the accretion rate vs. protostellar mass is shown for the fiducial model ($f_{\rm Kep} = 0.5$, $K' = 1$, $T_i = 25{,}000$ K) in the cases of "no feedback" and "with feedback." In the latter, the accretion efficiency is reduced as the H II region expands to r_g and beyond. However, accretion is allowed to continue from directions that are shadowed by the disk photosphere. The disk structure and protostellar structure and feedback are calculated self-consistently given the evolution in $\dot{m}_*$. Also shown is the photoevaporative mass-loss rate, $\dot{m}_{\rm evap}$, which starts once the H II region has broken out in the equatorial direction and grows as the ionizing flux increases. We see that this mass-loss rate becomes greater than the accretion rate at $m_* \simeq 137\ M_\odot$, and we identify this mass scale as our best estimate of initial mass scale of the first stars. [*See the electronic edition of the Journal for a color version of this figure.*]

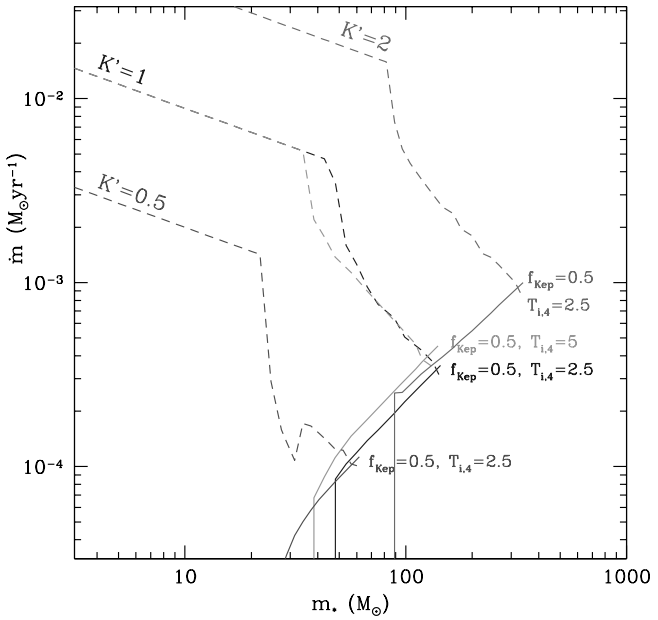

FIG. 9.—Feedback-limited accretion: effect of ionized gas temperature and accretion rate. The fiducial model ($f_{\rm Kep} = 0.5$, $K' = 1$, $T_{i,4} = 2.5$ K) shown in Fig. 8 is compared to models in which one parameter has been changed: a model with $T_{i,4} = 5$ and two models with $K' = 0.5$ and 2. The dashed lines show the accretion rate to the star, $\dot{m}_*$, and the solid lines show the photoevaporative mass-loss rate, $\dot{m}_{\rm evap}$. The change in temperature causes relatively minor differences, while the change in K', equivalent to a change in $\dot{m}_*$ of factors of 4.4 above and below the fiducial level, leads to roughly a factor of 2.4 change in the final stellar mass. Note that the increase in $\dot{m}_*$ for the $K' = 0.5$ case at around 35 $M_\odot$ is due to a thickening of the inner accretion disk as the star contracts down to its main-sequence configuration and assumes that material at large distances still remains to be accreted in the enlarged shadowed region. [*See the electronic edition of the Journal for a color version of this figure.*]

the total mass loss by a factor of 1.5. On the other hand, radiation pressure due to electron scattering reduces the effective mass by a factor $\phi_{\rm Edd} \sim 0.3$ (eq. [40]). Since the mass-loss rate scales as the square root of the gravitational mass, this reduction approximately cancels the increase due to mass loss from the inner disk. We therefore adopt the Hollenbach et al. (1994) estimate of $\dot{m}_{\rm evap}$ for our analytic and numerical estimates.

Accretion onto the star will cease shortly after the photoevaporation rate exceeds the accretion rate onto the star-disk system, which is given by equation (9). From equation (68), we find that the resulting maximum stellar mass is

$$\max m_{*f,2} = 6.3 \frac{\epsilon_{*d}^{28/47} \bar{\epsilon}_{*d}^{12/47} \phi_S^{14/47} K'^{60/47}}{(1+f_d)^{26/47}} \left(\frac{2.5}{T_4}\right)^{0.24}. \quad (69)$$

Recall that ϵ_{*d} is the instantaneous star formation efficiency, i.e., the ratio of the accretion rate onto the star to the rate that would have occurred in the absence of feedback. In the present case, this ratio is just the shadowing factor, $f_{\rm sh}$, introduced in the last section. In the numerical solution described below, we keep track of ϵ_{*d} as a function of time; for the analytic case, we make the simple approximation that the shadowing sets in when the stellar mass reaches m_1, so that $\epsilon_{*d} = 1$ until the mass of the central star reaches m_1 and $\epsilon_{*d} = f_{\rm sh}$ thereafter. It is then straightforward to show that

$$\bar{\epsilon}_{*d} = \frac{f_{\rm sh}}{1 - (1 - f_{\rm sh})(m_1/m_{*d})}, \quad (70)$$

provided that $m_{*d} \geq m_1$. Note that the average efficiency $\bar{\epsilon}_{*d} = 1$ at the onset of shadowing ($m_{*d} = m_1$) and that $\bar{\epsilon}_{*d} \rightarrow f_{\rm sh}$ at late times $m_{*d} \gg m_1$. Normalizing $f_{\rm sh}$ to a typical value of 0.2 from the results of § 7 and allowing for smaller accretion rates due to feedback, we find

$$\max m_{*f,2} = 1.45 K'^{60/47} \left(\frac{2.5}{T_4}\right)^{0.24} \left(\frac{f_{\rm sh}}{0.2}\right)^{28/47} \left(\frac{\bar{\epsilon}_{*d}}{0.25}\right)^{12/47}, \quad (71)$$

where we have set the ionizing luminosity factor $\phi_S = 1$ and the disk mass fraction $f_d = \frac{1}{3}$; we have normalized $\bar{\epsilon}_{*d}$ to a value of 0.25, which is approximately correct for $K' = 1$ and for $m_1 \simeq 50\ M_\odot$ as found in § 5.1.2 and $m_{*d} = 200\ M_\odot$. This analytic estimate therefore suggests that for the fiducial case ($K' = 1$) the mass of a first-generation star should be of order 140 $M_\odot$. We now confirm this with more accurate numerical integrations.

We evaluate the photoevaporative mass-loss rate in our numerical model with feedback (Fig. 8). The accretion rate is reduced as the H II region, with $T = 2.5 \times 10^4$ K, expands to r_g and beyond, although accretion is assumed to continue from directions shielded by the photosphere of the accretion disk. The disk and protostellar structure and feedback are calculated self-consistently given this evolution in the accretion rate. Beyond about 45 $M_\odot$ the accretion efficiency starts to be reduced below unity. By about 137 $M_\odot$ the evaporative mass-loss rate has become greater than the accretion rate and we then expect very limited growth of the protostar. We identify this mass scale as our fiducial estimate for the initial mass of the first stars. At this stage

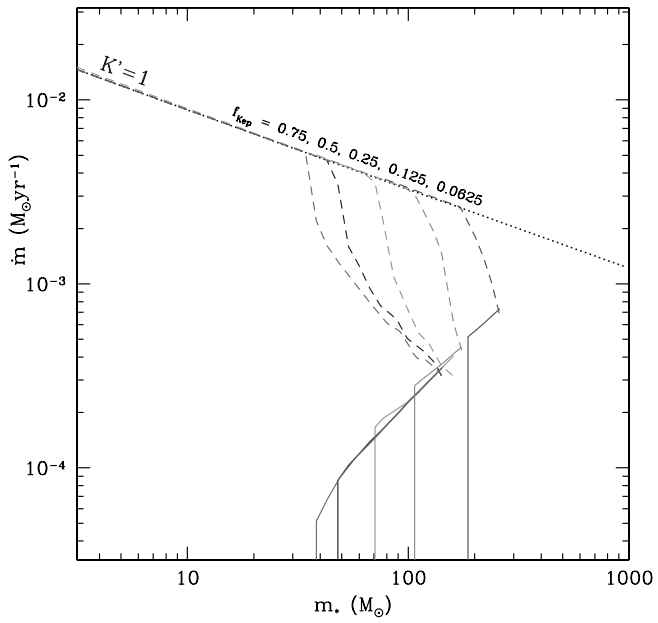

FIG. 10.—Feedback-limited accretion: effect of rotation. The fiducial model ($f_{\rm Kep} = 0.5$, $K' = 1$, $T_{i,4} = 2.5$ K) shown in Fig. 8 is compared to models in which only the rotation parameter $f_{\rm Kep}$ has been changed: $f_{\rm Kep} = 0.0625, 0.125$, 0.25, and 0.75. Smaller rotation parameters result in higher polar gas densities in the infall envelope and thus delayed H II region breakout (Fig. 5). However, for $f_{\rm Kep} \gtrsim 0.25$ this has relatively little effect on the final mass, which is set by disk photoevaporation (note the convergence of the $f_{\rm Kep} = 0.25, 0.5$, and 0.75 models). At smaller rotation parameters the process of H II region breakout plays an important role in setting the mass scale at which the accretion rate is truncated to be smaller than the photoevaporative mass-loss rate. [*See the electronic edition of the Journal for a color version of this figure.*]

$f_{\rm sh} \simeq 0.19$ and $\phi_S = 1.37$.[5] This estimate of the mass at which accretion ends agrees well with the analytic estimate of equation (71).

We investigate the sensitivity of this result to the ionized gas temperature by setting this equal to 50,000 K (Fig. 9). This causes the H II region to break out sooner and the disk photoevaporative mass-loss rate to be higher. However, with the other parameters unchanged ($K' = 1$, $f_{\rm Kep} = 0.5$), this has only a modest effect on the final mass, reducing it from 137 to 120 $M_\odot$.

We also consider the effect of changing the entropy parameter of the initial core by factors of 2 to higher and lower values ($K' = 0.5, 2$) (Fig. 9). This corresponds to a change in accretion rate of factors of 4.4 since $\dot{m}_* \propto (K')^{15/7}$. H II region breakout is accelerated/delayed by about a factor of 2 in protostellar mass by these changes. The final stellar mass set by disk photoevaporation shows a slightly broader range of factors of 2.4 smaller/greater than the fiducial value. This is consistent with equation (69), which would predict a change of a factor of 2.4 if the disk thickness was constant and accretion ionizing luminosity negligible.

Finally, we explore the effect of changing the core rotation. Figure 10 shows models with $f_{\rm Kep} = 0.0625$, 0.125, 0.25, 0.5, and 0.75 for $K' = 1$ and $T_i = 25{,}000$ K. Cores with higher rotation rates have lower densities in the infall envelope near the star so the H II region can break out more easily. However, for rotation parameters $f_{\rm Kep} \gtrsim 0.25$ this makes little difference to the final mass, which is set by the balance between (inner) disk-shadowed accretion and photoevaporative mass loss. For smaller rotation parameters ($f_{\rm Kep} \lesssim 0.125$) the process of H II region breakout does play an important role in setting the mass scale at which the accretion rate is truncated to be smaller than the photoevaporative mass-loss rate. However, given the results of numerical simulations of primordial core formation (O'Shea & Norman 2007), it appears that these low values of rotation are very rare.

[5] Note that only about 10% of this excess H-ionizing photon production rate is due to accretion. The remainder is due to our assumption that the spectrum of the protostar can be approximated as a blackbody, rather than the more detailed stellar atmosphere models of Schaerer (2002).

8. CONCLUSIONS

Recent numerical studies have indicated that the initial conditions for primordial star formation are dense, massive gas cores in approximate hydrostatic and virial equilibrium. These physical properties are set mostly by the microphysics of H_2 cooling and not by the initial cosmological density perturbations.

We have described the rate of collapse of these gas cores as a function of the entropy parameter of the gas, K, and the amount of mass that already collapsed. This accretion rate is very large, so that once an optically thick protostellar core forms, the star grows very quickly.

We have developed a simplified method for modeling protostellar evolution and applied the appropriate accretion rate for primordial protostars. The method allows for the treatment of accretion of gas with angular momentum, so that part of the accretion occurs via a disk. Using a realistic degree of rotation for the initial gas core, we find that, after the protostar has grown to about a solar mass, essentially all of the accretion flow is via the disk and conditions at the protostar are optically thin, in contrast to the spherical case. This means that the radiation field that the accretion envelope is exposed to is significantly hotter so that ionization and FUV radiation feedback can become important.

We considered the impact of the protostellar feedback on the infalling envelope. Again rotation is important because it modifies the density distribution in the vicinity of the star. First, we discussed the effects of photodissociation of H_2, the primary coolant. We showed that this does not stop accretion if the protostar has already begun to form, but it can suppress star formation in the vicinity (cf. Glover & Brand 2001). Next, we considered radiation pressure feedback due to resonant scattering of FUV radiation in the Lyα damping wings. As a result of the high column densities of neutral gas around the H II region, this radiation is trapped and the pressure amplified by large factors. This radiation pressure becomes larger than the ram pressure of the infalling gas in the polar directions for stellar masses of order 20 $M_\odot$. However, once the infall is reversed at the poles, the Lyα photons can escape and the accretion in other directions proceeds unimpeded. We then considered the growth of the ionized region. Once the expansion velocity of this region exceeds the free-fall velocity, the accretion is halted. This typically occurred at about 50–100 $M_\odot$, although it took much larger masses for cases with little angular momentum. The ionized gas is confined to the region above the disk, however, so accretion can continue in the shadow of the disk. Evaluating this, we found that shadowing permitted accretion to continue at a rate of about 20%–30% of that in the absence of the H II region. Allowing for photoevaporation of the disk, we found that the final stellar mass is about 140 $M_\odot$ in the fiducial case.

Table 1 summarizes how the mass scales set by protostellar feedback depend on model parameters. The final mass of a Population III.1 star depends fairly sensitively on the entropy parameter of the accreting gas [i.e., approximately as $(K')^{1.3}$], which in turn determines the overall accretion rate to the star+disk, but not very much on core rotation (for $f_{\rm Kep} \gtrsim 0.25$) or ionized gas temperature (T_i). At very low values of core rotation, H II region breakout is delayed until high protostellar masses, at which

TABLE 1
Mass Scales of Population III.1 Protostellar Feedback

K'	$f_{\rm Kep}$	T_i (10^4 K)	$m_{*,\rm pb}$[a] ($M_\odot$)	$m_{*,\rm eb}$[b] ($M_\odot$)	$m_{*,\rm evap}$[c] ($M_\odot$)
1	0.5	2.5	45.3	50.4	137[d]
	0.75	2.5	37	41	137
	0.25	2.5	68	81	143
	0.125	2.5	106	170	173
	0.0626	2.5	182	330[e]	256
	0.5	5.0	35	38	120
	0.25	5.0	53.0	61	125
0.5	0.5	2.5	23.0	24.5	57
2.0	0.5	2.5	85	87	321

[a] Mass scale of H II region polar breakout.
[b] Mass scale of H II region near-equatorial breakout.
[c] Mass scale of disk photoevaporation limited accretion.
[d] Fiducial model.
[e] This mass is greater than $m_{*,\rm evap}$ in this case because it is calculated without allowing for a reduction in $\dot{m}_*$ during the evolution due to polar H II region breakout.

point the disk photoevaporation rate soon exceeds the residual disk-shadowed accretion rate. However, these small values of $f_{\rm Kep}$ are not very likely to occur in nature.

The final masses predicted by our model overlap the range of masses necessary to produce pair instability supernovae, 140–260 $M_\odot$ (Heger & Woosley 2002). Rotation may lower these limits (S. Woosley 2007, private communication). The lack of the expected nucleosynthetic signature of such supernovae in the abundance patterns of very metal-poor halo stars (Tumlinson et al. 2004) could indicate that such massive Population III.1 stars were relatively rare or that they tended to enrich regions not probed by typical halo stars, perhaps the centers of larger galactic halos. The conclusion by Scannapieco et al. (2006) that Population III star formation should be fairly widespread in regions now probed by Galactic halo stars can be reconciled with the abundance pattern observations if most of this star formation leads to either Population III.1 stars from relatively low entropy ($K' \lesssim 1$) gas cores or Population III.2 stars that also have a mass scale below the pair instability threshold (see also the study by Greif & Bromm 2006). Further work is required to determine the range of prestellar core parameters, primarily K' and $f_{\rm Kep}$, exhibited in cosmological simulations, in order to predict the frequency of pair instability supernovae.

One may ask how the feedback mechanisms we have considered relate to those that operate in contemporary massive star formation. We note that the maximum mass attained in our fiducial model of Population III.1 star formation is very similar to that inferred observationally in local massive star clusters (e.g., Figer 2005). However, after decades of study, it remains unclear whether the maximum mass of stars forming today is set by feedback or instabilities in very massive stars (Larson & Starrfield 1971). Here we have argued that the maximum mass of primordial stars is set by feedback. The primary differences in the feedback processes then and now are as follows:

1. *Dust*.—In contemporary star-forming regions, dust destroys Lyα photons, eliminating them as a significant pressure. On the other hand, the dust couples the pressure of the UV continuum radiation to the gas very effectively, and it remains to be determined whether this limits the final mass of the star; e.g., Yorke & Sonnhalter (2002) find that it does, whereas Krumholz et al. (2005a) have not found evidence that it does. Dust also affects the evolution of H II regions, absorbing a significant fraction of the ionizing photons in dense H II regions (Spitzer 1978), thereby reducing the H II feedback discussed in § 5 and the photoevaporation in § 7.

2. *Magnetic fields*.—In contemporary protostars, magnetic fields drive powerful protostellar winds that drive away a significant fraction of the core out of which the star is forming (Matzner & McKee 2000). The cavities created by these winds allow radiation to escape from the vicinity of the protostar, significantly reducing the radiation pressure (Krumholz et al. 2005b). Tan & Blackman (2004) considered the influence of such outflows on Population III.1 cores, concluding that the instantaneous efficiency of accretion could be reduced by a factor of about 2 from the no-feedback case in an isotropic core by the time the star reached 100 $M_\odot$. However, these outflows would not confine ionizing feedback from the star at these masses; so much of the gas that could be expelled by outflows would have already been disrupted by H II region breakout. We conclude that outflows would have a relatively minor effect on the results presented here and that the masses of the first stars are mostly influenced by radiative feedback. See Tan & McKee (2008) for further discussion.

3. *Stellar temperatures and luminosities*.—Primordial stars were significantly hotter than contemporary stars, resulting in significantly greater ionizing luminosities. In addition, the accretion rates of primordial massive stars are much greater, at least initially, than those of contemporary massive stars (McKee & Tan 2002, 2003). Future calculations will show whether feedback can be as effective in setting the maximum mass of contemporary stars as we have argued that it is for primordial stars.

We thank T. Abel, F. Adams, V. Bromm, B. Draine, J. Goodman, D. McLaughlin, G. Meynet, B. O'Shea, J. Ostriker, S. Phinney, E. Scannapieco, D. Whalen, and N. Yoshida for helpful discussions. During the course of this work J. C. T. has been supported by a Spitzer-Cotsen Fellowship from Princeton University, by a Zwicky Fellowship from ETH Zürich, and by NSF CAREER grant AST 06-45412. The research of C. F. M. is supported by NSF grants AST 06-06831 and PHY-0551164 and by the DOE through grant DE-FC02-06ER41453.

APPENDIX A

LINE PROFILE WITH RAYLEIGH SCATTERING

A complication that occurs in our problem is that the column density can become so large that Rayleigh scattering is important. From Jackson (1975, p. 802), we find that in general the scattering cross section can be expressed as

$$\sigma(\nu) = \bar{\sigma}\Delta\nu_D\phi_{1\nu}, \tag{A1}$$

where

$$\bar{\sigma} \equiv \frac{1}{\Delta\nu_D}\int \sigma(\nu)\, d\nu, \tag{A2}$$

$$\phi_{1\nu} = \left(\frac{1}{\pi}\right)\frac{\left(4\nu^4/\nu_0^2\right)(\Gamma/4\pi)}{\left(\nu_0^2-\nu^2\right)^2 + \left(4\nu^6/\nu_0^4\right)(\Gamma/4\pi)^2}, \tag{A3}$$

and Γ is the total spontaneous transition rate out of the upper and lower levels of the transition. For the simple case of a two-level atom (which can be used for Lyα), $\Gamma = A_{21}$ is the Einstein A-coefficient for the transition. Physically, $\phi_{1\nu}$ is the line profile for scattering by an individual atom; the line profile for a gas, ϕ_ν, is obtained by convolving $\phi_{1\nu}$ with a Maxwellian distribution.

We now develop an accurate approximation for $\phi_{1\nu}$. Defining

$$f(\nu) \equiv \frac{4\nu^4}{\nu_0^2(\nu_0+\nu)^2}, \tag{A4}$$

which is unity at line center, we have

$$\phi_{1\nu} = \left(\frac{1}{\pi}\right)\frac{(\Gamma/4\pi)f(\nu)}{\Delta\nu^2 + (\nu/\nu_0)^2(\Gamma/4\pi)^2 f(\nu)} \tag{A5}$$

$$\simeq \left(\frac{1}{\pi}\right)\frac{(\Gamma/4\pi)f(\nu)}{\Delta\nu^2 + (\Gamma/4\pi)^2}. \tag{A6}$$

The approximation of dropping the factor $(\nu/\nu_0)^2 f(\nu)$ in the denominator has an error of order $\Gamma/(4\pi\nu_0) = A_{21}/(4\pi\nu_0)$, which is less than 10^{-6} for Lyα. At low frequencies ($\nu \ll \nu_0$), we have $\phi_{1\nu} \propto f(\nu) \propto \nu^4$, the standard frequency scaling for Rayleigh scattering.

In terms of the normalized frequency shift $x \equiv \Delta\nu/\Delta\nu_D$, we have $\sigma(x) = \bar{\sigma}\phi_{1x}$, where

$$\phi_{1x} = \frac{1}{\pi}\left[\frac{af(\nu)}{a^2+x^2}\right] \tag{A7}$$

and $a \equiv \Gamma/(4\pi\Delta\nu_D)$. For Ly$\alpha$, $a = 6.04\times10^{-4}/\Delta v_{D,6}$, where $\Delta v_{D,6} \equiv \Delta v_D/(10^6\ \mathrm{cm\ s^{-1}})$. The line profile for a gas, ϕ_x, is the same as this in the line wings ($x \gg 1$). We conclude that the line profile in the damping wings is given by

$$\phi_x \simeq \frac{af(\nu)}{\pi x^2} \qquad (x \gg 1). \tag{A8}$$

The correction to the usual expression for the damping profile is given by the factor $f(\nu)$, which drops to 0.5 at $\nu = 0.80\nu_0$. The relation between ν and x is given by

$$\frac{\nu}{\nu_0} = 1 + \frac{x\Delta\nu_D}{\nu_0} = 1 + 3.33\times10^{-5}\Delta v_{D,6}\, x, \tag{A9}$$

where the final expression is for Lyα.

The optical depth at a frequency labeled by x is $\tau_x = \bar{\tau}_{\rm eff}\phi_x$. For Ly$\alpha$,

$$\bar{\tau}_{\rm eff} = 1.34\times10^{-13}N_{\rm eff}/\Delta v_{D,6} \tag{A10}$$

(Neufeld 1990), where $N_{\rm eff}$ is the effective column density of H I (see eq. [20]). Thus, in the damping wings of Lyα we have

$$\tau_x = 2580\left[\frac{N_{\rm eff,20}f(\nu)}{\Delta v_{D,6}^2 x^2}\right] \qquad (x \gg 1). \tag{A11}$$

The frequency $0.8\nu_0$, where $f(\nu) = 0.5$, corresponds to $x = 6000/\Delta v_{D,6}$. In order to have optical depth unity at this point, the column density must be $N_{\rm eff} \sim 3\times10^{24}$.

APPENDIX B

ENHANCEMENT OF Lyα INTENSITY IN AN OPTICALLY THICK MEDIUM

Here we derive the increase in Lyα intensity relative to the optically thin limit due to the trapping of photons in regions of high column densities, such as the neutral gas around the protostellar H II region. This factor was used in § 4 for the calculation of the Lyα radiation pressure feedback, and some of the symbols in this appendix are defined there. We first consider the case of pure scattering and then include the effect of destruction by two-photon emission.

B1. CASE OF PURE SCATTERING

We follow the treatment of Neufeld (1990), which extended earlier work by Harrington (1973). He considered a uniform, planar slab of thickness $2\bar{\tau}_L$, with the origin at the center of the slab. A planar source of photons located at $\bar{\tau}_s$ produces an incident flux F_i in each direction; he normalized to $F_i = \frac{1}{2}$. We assume that there is no absorption. First, consider the case in which the photons are injected at line center ($x_i = 0$). The frequency-integrated intensity at a point $\bar{\tau}$ in the slab is

$$\frac{J(\bar{\tau}; x_i = 0)}{2F_i} = \left(\frac{3}{2}\right)^{1/2}\left(\frac{4a\bar{\tau}_L}{\pi}\right)^{1/3}\left[\mathcal{F}\left(\frac{\bar{\tau} - \bar{\tau}_s'}{2\bar{\tau}_L}\right) - \mathcal{F}\left(\frac{2\bar{\tau}_L - \bar{\tau} - \bar{\tau}_s'}{2\bar{\tau}_L}\right)\right], \tag{B1}$$

where

$$\mathcal{F}(w) = \frac{\sqrt{6}\Gamma(1/3)}{12\pi^{7/3}}\sum_{n=1}^{\infty}\frac{\cos(n\pi w)}{n^{4/3}}. \tag{B2}$$

In general,

$$\bar{\tau}_s' \equiv \bar{\tau}_s\left(1 - \frac{2}{3\bar{\tau}_L\phi_i}\right), \tag{B3}$$

where $\phi_i = \phi(x_i)$ is the line profile at the injection frequency; we have assumed that the photons are injected at line center, so that $\phi_i = \phi_0$ is not small. We further assume that $\bar{\tau}_s' \simeq \bar{\tau}_s$, which is valid provided that $\Delta\bar{\tau}_s \equiv \bar{\tau}_L - \bar{\tau}_s \gg 1$, i.e., the source is not too near the edge of the slab.

For the case in which the source is at the center of the slab ($\bar{\tau}_s = 0$), the intensity at the center of the slab is

$$J_s(x_i = 0) = J(0; x_i = 0) = \left(2^{4/3} - 1\right)\left[\frac{\Gamma(1/3)\zeta(4/3)}{2^{2/3}\pi^{8/3}}\right](a\bar{\tau}_L)^{1/3}F_i = 0.4362(a\bar{\tau}_L)^{1/3}F_i, \tag{B4}$$

as originally found by Harrington (1973). This has the same scaling as expected from the heuristic argument given in § 4: in the absence of any scattering, the mean intensity would be $J = F_i/2\pi$ (assuming isotropic emission), so the mean intensity is indeed enhanced by a factor of order $(a\bar{\tau}_L)^{1/3}$.

Next, consider the case in which the source is near the edge of the slab but, in view of the smallness of the Lyα mean free path, still at a large optical depth from the edge ($\bar{\tau} \gg \Delta\bar{\tau}_s \gg 1$). The maximum intensity occurs at $\bar{\tau}_s$ and is proportional to

$$\mathcal{F}(0) - \mathcal{F}\left(\frac{\Delta\bar{\tau}_s}{\bar{\tau}_L}\right) = \frac{\sqrt{6}\Gamma(1/3)}{12\pi^{7/3}}\sum_{n=1}^{\infty}\frac{1 - \cos(n\pi\Delta\bar{\tau}_s/\bar{\tau}_L)}{n^{4/3}}. \tag{B5}$$

Approximating the sum by

$$2\int_0^{\infty} dn\, n^{-4/3}\sin^2\left(\frac{n\pi\Delta\bar{\tau}_s}{2\bar{\tau}_L}\right) = -\Gamma\left(-\frac{1}{3}\right)\cos\left(\frac{\pi}{6}\right)\left(\frac{\pi\Delta\bar{\tau}_s}{\bar{\tau}_L}\right)^{1/3} \tag{B6}$$

(Gradshteyn & Ryzhik 1965, p. 447), we find

$$J_s(x_i = 0) = 0.518(a\Delta\bar{\tau}_s)^{1/3}F_i = 0.411(a\bar{\tau}_{\rm eff})^{1/3}F_i, \tag{B7}$$

where the effective optical depth is $\bar{\tau}_{\rm eff} = 2\Delta\bar{\tau}_s$ (eq. [20]) for the case in which the source is close to one edge. Note that this agrees quite well with our *Ansatz*, equation (20), since when the result for a source near the edge is expressed in terms of $\bar{\tau}_{\rm eff}$, it is nearly the same as that for a source near the center (eq. [B4]).

Neufeld's results are valid only in the limit in which $a\bar{\tau}_L \gtrsim 10^3$, so that the transfer is completely determined by the damping wings. Hummer & Kunasz (1980) show that for smaller optical depths, there is an intermediate regime in which J/F_i is about constant. They define a quantity $\rho_{\rm HK} \equiv \rho\bar{\kappa}D/\bar{\tau}_L$, where the density ρ is assumed to be constant and where D is the mean distance traveled by an escaping photon. As shown by Ivanov (1970), this is $(4\pi/2\bar{\tau}_L F_i)\int J\, d\bar{\tau}$, which in turn is proportional to J_s/F_i. For the case $1 \gtrsim \Delta v_{D,6} \gtrsim 0.1$ (corresponding to 10^4 K $\gtrsim T \gtrsim 10^2$ K), the results of Hummer & Kunasz (1980) imply that $\rho_{\rm HK}$ and therefore J_s/F_i are within about 0.1 dex of their values at $a\bar{\tau}_L = 450$ for $10^3 \gtrsim a\bar{\tau}_L \gtrsim 1$. We assume that the same behavior obtains in terms of $\bar{\tau}_{\rm eff}$ for a source near the edge of the slab. Thus, for $\bar{\tau}_{\rm eff} \gtrsim 1/a = 1660\Delta v_{D,6}$, we have

$$\left|\frac{J_s}{F_i}\right|_{x_i} \simeq \frac{0.411(a\bar{\tau}_{\rm eff})^{1/3}}{\min\left[1,\ (a\bar{\tau}_{\rm eff}/450)^{1/3}\right]}. \tag{B8}$$

For $450 \gtrsim a\bar{\tau}_{\rm eff} \gtrsim 1$, this gives $J_s/F_i \simeq 3.15$. The condition $a\bar{\tau}_{\rm eff} \gtrsim 1$ for the validity of equation (B8) corresponds to column densities $N_{\rm eff} \gtrsim 10^{16}\Delta v_{D,6}^2$ cm^{-2}.

This result is valid for Lyα photons produced by the H II region, since such photons are very near line center. Stellar FUV photons are not restricted to line center, but fortunately Neufeld has evaluated the intensity for an arbitrary injection frequency. Since his results for this case are somewhat complicated, we evaluate the intensity far from line center and then smoothly join the result onto the result we have found above. If the injection frequency is large compared to the diffusion frequency [$x_i \gg (a\bar{\tau}_{\rm eff})^{1/3}$], then the photons scatter approximately coherently. The intensity in this case can be found either from Neufeld's general results[6] or from a simple solution to the radiative transfer equation. We normalize the injection frequency,

$$\hat{x}_i \equiv \frac{x_i}{(a\bar{\tau}_{\rm eff})^{1/3}}, \tag{B9}$$

so that photons injected with $\hat{x}_i \ll 1$ are in the diffusion regime and those with $\hat{x}_i \gg 1$ are in the coherent scattering regime. In the latter case, we find

$$\left|\frac{J_{s,\rm iso}}{F_i}\right|_{x_i} = \frac{3}{4\pi}\phi_i\bar{\tau}_{\rm eff} = \left(\frac{3}{4\pi^2}\right)\frac{(a\bar{\tau}_{\rm eff})^{1/3}f(\nu)}{\hat{x}_i^2} \qquad (\hat{x}_i \gg 1), \tag{B10}$$

where $f(\nu)$ is the Rayleigh scattering factor defined in equation (A4). We have put the subscript "iso" on the mean intensity to indicate that it has been derived under the assumption that the medium is optically thick at the frequency x_i so that the photons are isotropic. Sufficiently far in the line wings, equation (B10) shows that $J_{s,\rm iso}$ goes to zero. This approximation is developed further in Appendix C. If several lines contribute to the opacity at a given frequency, then the right-hand side of equation (B10) should be summed over the lines, since it is the total opacity that governs the mean intensity.

We are now in a position to join the result for the frequency diffusion (eq. [B7]) to that for coherent scattering in the far wings of the line (eq. [B10]). Taking the harmonic mean of these results, we obtain an expression that is approximately valid for all injection frequencies:

$$\left|\frac{J_{s,\rm iso}}{F_i}\right|_{x_i} \simeq \frac{0.411(a\bar{\tau}_{\rm eff})^{1/3}}{\min\left[1,\ (a\bar{\tau}_{\rm eff}/450)^{1/3}\right] + 5.41[\hat{x}_i^2/f(\nu)]}. \tag{B11}$$

Note that the numerical coefficient has been chosen to agree with the case of a source near the edge of a cloud, which is the one most relevant to our problem. The intensity is half that at line center for an injection frequency $\hat{x}_i = 0.43$ [for $a\bar{\tau}_{\rm eff} > 450$ and $f(\nu) \simeq 1$].

B2. EFFECT OF TWO-PHOTON EMISSION

In the absence of dust or molecular hydrogen, the dominant destruction processes for Lyα photons are collisional de-excitation (which we ignore) and two-photon emission following a collisional transition from the $2p$ to the $2s$ state. Lyα photons can also be destroyed by photoionization out of the $n = 2$ state, but since another Lyα photon is created after the ion recombines, the net destruction by this process vanishes.

Consider a one-dimensional slab of gas with a central source of Lyα photons. Let ϵ be the probability of two-photon emission per scattering. Then in the limit of large optical depth, the mean intensity at the source is (Harrington 1973)

$$J_s(x_i = 0) = 0.396(a/\epsilon)^{1/3}F_i, \tag{B12}$$

which is quite close to the result with no absorption (eq. [B4]) with the replacement $\bar{\tau}_L \rightarrow 1/\epsilon$. Thus, two-photon emission prevents the mean intensity from increasing once $\epsilon\bar{\tau}_L \gtrsim 1$. We join this result onto the expression for the case in which the source is not at the center and there is no absorption (eq. [B8]) by writing

$$J_s(x_i = 0) = \frac{0.411(a\bar{\tau}_{\rm eff})^{1/3}}{\min\left[1,\ (a\bar{\tau}_{\rm eff})^{1/3}\right] + \Gamma}, \tag{B13}$$

with

$$\Gamma = 1.04(\epsilon\bar{\tau}_{\rm eff})^{1/3}. \tag{B14}$$

To determine the destruction probability ϵ, we need to know the population of the $2s$ state. In statistical equilibrium, this is

$$\frac{n_{2s}}{n_{2p}} = \frac{1}{3}\left(\frac{1}{1 + n_{e,\rm cr}/n_e}\right), \tag{B15}$$

[6] The numerical coefficient in Neufeld's eq. (2.30) is too small by a factor of 3, as confirmed by the author (D. A. Neufeld 2003, private communication).

where

$$n_{e,\mathrm{cr}} \equiv \frac{A_{2s1s}}{q_{2s2p}} = 1.55 \times 10^4 \ \mathrm{cm}^{-3} \tag{B16}$$

is the critical density for the $2s \rightarrow 2p$ transition, $A_{2s1s} = 8.23\ \mathrm{s}^{-1}$ is the two-photon emission rate from the $2s$ state, and $q_{2s2p} = 5.31 \times 10^{-4}\ \mathrm{cm}^3\ \mathrm{s}^{-1}$ is the collisional rate coefficient for electron and proton collisions from the $2s$ state to the $2p$ state (Osterbrock 1989). Collisional de-excitation from $2s$ to $1s$ is much slower and may be neglected in determining this population ratio. The probability per scattering of destroying a Lyα photon by two-photon emission is then

$$\epsilon = \frac{n_{2s} A_{2s1s}}{n_{2p} A_{2p1s}} = \frac{4.4 \times 10^{-9}}{1 + n_{e,\mathrm{cr}}/n_e}. \tag{B17}$$

Collisional de-excitation to the $1s$ level competes with this process for $n_e \gtrsim 10^8\ \mathrm{cm}^{-3}$, but we assume that n_e is less than this so that we can ignore this process. Inserting this result into equation (B14), we find that the factor that gives the effect of two-photon emission is

$$\Gamma = \frac{0.405\left(N_{\mathrm{eff},20}/\Delta v_{D,6}\right)^{1/3}}{\left(1 + n_{e,\mathrm{cr}}/n_e\right)^{1/3}}. \tag{B18}$$

We see that at high electron densities ($n_e \gg n_{e,\mathrm{cr}}$), two-photon emission reduces the Lyα intensity by a factor that depends only on the column density and the velocity dispersion. Although the large column densities of H I needed to make this process important occur in regions of neutral hydrogen, one can show that photoionization out of the $n = 2$ state is generally sufficiently effective that $n_e \gtrsim n_{e,\mathrm{cr}}$ in the H I just outside the H II regions of massive primordial stars. As a result, we have

$$\Gamma \simeq 0.405\left(N_{\mathrm{eff},20}/\Delta v_{D,6}\right)^{1/3}. \tag{B19}$$

This destruction process operates only for photons that can diffuse to the center of the line, which is where most of the scatterings take place. For stellar FUV photons, we assume that this occurs only for photons within a frequency range $(a\bar{\tau}_{\mathrm{eff}})^{1/3}\Delta\nu_D$, or $|\hat{x}_i| < 1$, so that Γ depends on $\hat{x}_i$:

$$\Gamma(\hat{x}_i) = \begin{cases} \Gamma, & |\hat{x}_i| < 1, \\ 0, & |\hat{x}_i| > 1. \end{cases} \tag{B20}$$

B3. THE BLACKBODY CONSTRAINT

We have one last constraint to impose: the intensity we calculate must be less than the appropriate blackbody intensity B_ν. The Lyα photons produced by the H II region have a complicated line profile that is concentrated in a frequency range $\sim 2(a\bar{\tau}_{\mathrm{eff}})^{1/3}\Delta\nu_D$. For these photons, we require that the intensity in this frequency range be less than that of a blackbody at the temperature of the H II region,

$$J_{\alpha,\mathrm{H\,II}} = \min\left\{ 2(a\bar{\tau}_{\mathrm{eff}})^{1/3}\Delta\nu_D B_{\nu_\alpha}(T_{\mathrm{H\,II}}),\ \frac{0.411(a\bar{\tau}_{\mathrm{eff}})^{1/3} F_{\alpha,\mathrm{H\,II}}}{\min\left[1,\ (a\bar{\tau}_{\mathrm{eff}}/450)^{1/3}\right] + \Gamma} \right\}. \tag{B21}$$

For stellar photons, the intensity is limited by the blackbody intensity at the stellar surface, $B_\nu(T_*) = F_{\nu *}/\pi$:

$$J_{\alpha *,\mathrm{iso}} = \int d\nu_i \min\left\{ B_{\nu_i}(T_*),\ \frac{0.411(a\bar{\tau}_{\mathrm{eff}})^{1/3} F_i(\nu_i)}{\min\left[1,\ (a\bar{\tau}_{\mathrm{eff}}/450)^{1/3}\right] + 5.41[\hat{x}_i^2/f(\nu)] + \Gamma(\hat{x}_i)} \right\}. \tag{B22}$$

The subscript "iso" indicates that $J_{\alpha *,\mathrm{iso}}$ is that part of the stellar radiation that has been isotropized by scattering (see Appendix C). The factor in the denominator ensures that although the integral is taken over the entire spectrum of the star, it is only that part near the resonance line that contributes.

APPENDIX C

ESTIMATE OF THE RADIATION PRESSURE

In opaque media, the force exerted by radiation can be treated as an isotropic pressure, just like gas pressure. If the medium is not opaque, however, the radiation pressure tensor is not diagonal, and radiation pressure does not behave like gas pressure. For example, in the optically thin limit, the radiation pressure declines as r^{-2}, yet the associated force per unit volume is negligible. Here we introduce an approximation to the radiation pressure tensor that separates out the isotropic part and show that the radiative force is the gradient of this pressure.

The radiative force per unit volume is

$$\boldsymbol{f}_{\rm rad} = -\nabla\cdot\boldsymbol{P}_{\rm rad} = \frac{1}{c}\rho\kappa\boldsymbol{F}, \tag{C1}$$

where $\boldsymbol{P}_{\rm rad}$ is the radiation pressure tensor (e.g., Shu 1991); for a frequency-dependent opacity, $\kappa\boldsymbol{F} = \int \kappa_\nu \boldsymbol{F}_\nu$. At large optical depths, the radiation field is nearly isotropic and the radiation pressure tensor becomes diagonal, $\boldsymbol{P}_{\rm rad} \rightarrow P_{\rm rad,\,iso}\boldsymbol{I}$. At small optical depths, the radiation is beamed and $\boldsymbol{P}_{\rm rad} \rightarrow (1/c)\boldsymbol{F}\hat{\boldsymbol{F}}$, where $\hat{\boldsymbol{F}}$ is a unit vector. (Note that in one dimension, the radiation is not purely beamed at small optical depth, so there is a numerical coefficient ≤ 1 in front of $\boldsymbol{F}$ in this expression.) We then have for all optical depths

$$\boldsymbol{P}_{\rm rad} \simeq P_{\rm rad,\,iso}\boldsymbol{I} + \frac{1}{c}\boldsymbol{F}\hat{\boldsymbol{F}}, \tag{C2}$$

and the radiative force is

$$\boldsymbol{f}_{\rm rad} = -\nabla\cdot\boldsymbol{P}_{\rm rad} \simeq -\nabla P_{\rm rad,\,iso} - \frac{1}{c}\hat{\boldsymbol{F}}\nabla\cdot\boldsymbol{F}. \tag{C3}$$

Here we have omitted the term $\boldsymbol{F}\cdot\nabla\hat{\boldsymbol{F}}$, which vanishes in the optically thin limit since then the flux does not change direction along a ray, and which is negligible in the optically thick limit even if the flux does change direction. In the case of pure scattering, or in a stellar atmosphere, we have $\nabla\cdot\boldsymbol{F} = 0$, so the radiative force is then

$$\boldsymbol{f}_{\rm rad} \simeq -\nabla P_{\rm rad,\,iso} = \frac{1}{c}\rho\kappa\boldsymbol{F} \qquad (\text{for } \nabla\cdot\boldsymbol{F} = 0). \tag{C4}$$

This is the case relevant to our problem. On the other hand, in the case of strong absorption, so that F decreases in a distance small compared to the radius, one cannot neglect the term $\hat{\boldsymbol{F}}\nabla\cdot\boldsymbol{F}$ in evaluating the force.

If $\boldsymbol{F}$ is known, then $P_{\rm rad,\,iso}$ can be determined from equation (C4) once a boundary condition is specified. We assume that there is a surface to the gas distribution. It follows that $\boldsymbol{f}_{\rm rad} \propto \kappa$ vanishes outside the surface, so that $P_{\rm rad,\,iso}$ must be constant there. Since the radiation pressure vanishes at infinity, it follows that the constant must be zero. We conclude that $P_{\rm rad,\,iso} = 0$ at the surface of the gas distribution.

At large optical depths, the energy density of the radiation is $u_{\rm rad} = 4\pi J/c = 3P_{\rm rad}$. We therefore define $u_{\rm rad,\,iso} \equiv 4\pi J_{\rm iso}/c \equiv 3P_{\rm rad,\,iso}$. Since $u_{\rm rad} \rightarrow F/c$ at small optical depths, we have $u_{\rm rad} \simeq u_{\rm rad,\,iso} + F/c$.

Under the assumptions of spherical symmetry and no net absorption ($\nabla\cdot\boldsymbol{F} = 0$), our formulation is equivalent to the closure approximation recommended by Shu (1991, pp. 43–44). He shows that the equation for the rr component of the radiation pressure tensor is

$$\frac{\partial P_{{\rm rad},\,rr}}{\partial r} + \frac{1}{r}\left(3P_{{\rm rad},\,rr} - u_{\rm rad}\right) = -\frac{1}{c}\rho\kappa F. \tag{C5}$$

Shu points out that $3P_{{\rm rad},\,rr} - u_{\rm rad} \simeq 2F/c$, since at high optical depths F is negligible and $P_{\rm rad} = u_{\rm rad}/3$, whereas at low optical depths $P_{{\rm rad},\,rr} = u_{\rm rad} = F/c$. With this approximation, the left-hand side of the equation becomes $\partial P_{{\rm rad},\,rr}/\partial r + 2F/cr$. Our formulation gives $P_{{\rm rad},\,rr} = P_{\rm rad,\,iso} + F/c$. Since we have assumed $\nabla\cdot\boldsymbol{F} = 0$, we have $\partial F/\partial r = -2F/r$ in the spherically symmetric case, so that equation (C5) reduces to equation (C4).

Recall that the Lyα radiation pressure, $P_{\rm rad,\,iso}$ in equation (22), was derived for a slab geometry. What is the appropriate value of the column density $N_{\rm eff}$ to use in this expression in a more realistic geometry? Here we determine the relation between a slab geometry and a spherical one; in Appendix D, we generalize this to nonspherical geometries. However, it must be borne in mind that the actual geometry of the infalling gas is far more complicated than can be represented by a simple analytic model.

What is the relation between the optical depth in one dimension and that in three dimensions that results in the same radiation pressure? Let $F \propto r^{-k_F}$, with $k_F = 0$ for slab geometry and $k_F = 2$ for spherical geometry. We assume that the density in the spherical case can be described by a power law, $\rho \propto r^{-k_\rho}$. For a constant opacity per unit mass, we therefore have

$$\frac{\partial P_{\rm rad,\,iso}}{\partial r} = -\frac{\rho_0\kappa F_0}{c}\left(\frac{r_0}{r}\right)^{k_F+k_\rho}, \tag{C6}$$

where r_0 is a fiducial radius and $\rho_0 \equiv \rho(r_0)$, etc. The optical depth from r to infinity in the spherical case is

$$\tau_{\rm 3D} = \frac{\rho\kappa r}{k_\rho - 1} \tag{C7}$$

for $k_\rho > 1$, so that the solution of equation (C6) is

$$P_{\rm rad,\,iso} = \left(\frac{k_\rho - 1}{k_\rho + k_F - 1}\right)\frac{F\tau}{c}. \tag{C8}$$

In order for the radiation pressure in the slab to be the same as that in a sphere for the same value of the flux, we require

$$\tau_{1D} = \left(\frac{k_\rho - 1}{k_\rho + 1}\right)\tau_{3D} = \frac{\rho\kappa r}{k_\rho + 1}. \tag{C9}$$

Since $\tau_{1D} = \mu_H \kappa N_{eff}$, we conclude that

$$N_{eff} = \frac{nr}{k_\rho + 1}. \tag{C10}$$

For a free-fall density variation, valid for $r \gtrsim r_d$, we have $k_\rho = 3/2$ so that $N_{eff} = \frac{2}{5}nr$; inside r_d, $k_\rho = \frac{1}{2}$ is a more accurate description, so that $N_{eff} = \frac{2}{3}nr$.

APPENDIX D

ANISOTROPIC OPTICAL DEPTH AND SUPERCRITICAL ACCRETION

In order to estimate how Lyα photons escape from the H II region around the protostar, we consider the following idealized problem: we assume that the radiation fills a cavity bounded by a thin, opaque shell of variable optical depth, $\tau(\boldsymbol{r})$. In this case, the flux at the surface of the shell is approximately normal to the surface, $\hat{\boldsymbol{F}} \simeq \hat{\boldsymbol{n}}$, and the radiation energy density is about constant in the interior of the shell. This model will be approximately valid for Lyα radiation once the H II region separates from the star, since the H II region provides a cavity in which the optical depth due to resonance line scattering is relatively small, so that the radiation becomes approximately uniform there. Equation (C4) then gives

$$\boldsymbol{F}(\boldsymbol{r}) \simeq -c\frac{dP_{rad,iso}}{d\tau(\boldsymbol{r})}\hat{\boldsymbol{n}} \simeq \frac{cP_{rad,iso}}{\tau(\boldsymbol{r})}\hat{\boldsymbol{n}}. \tag{D1}$$

Integration over the surface of the shell gives the luminosity:

$$L = \int \boldsymbol{F}\cdot\hat{\boldsymbol{n}}\, dA \simeq cP_{rad,iso}\int \frac{dA}{\tau(\boldsymbol{r})} = \frac{cP_{rad,iso}A}{\bar{\tau}_{eff}}, \tag{D2}$$

where A is the total area of the shell and $\bar{\tau}_{eff}$ is the harmonic mean optical depth:

$$\frac{1}{\bar{\tau}_{eff}} \equiv \frac{1}{A}\int \frac{dA}{\tau(\boldsymbol{r})}. \tag{D3}$$

For a spherical shell, this simplifies to

$$\frac{1}{\bar{\tau}_{eff}} = \frac{1}{4\pi}\int \frac{d\Omega}{\tau(\hat{\boldsymbol{r}})}. \tag{D4}$$

We can generalize this treatment to allow for the possibility that the optical depth is small in some directions. Consider the extreme case in which $\tau = 0$ over a small area δA, i.e., there is a small hole in the shell. The flux emerging from this area is π times the specific intensity, which is the same as the mean intensity J in the cavity. We therefore find

$$F(\boldsymbol{r}) = \pi J = \frac{cu_{rad}}{4} = \frac{3cP_{rad}}{4} \simeq \frac{3cP_{rad,iso}}{4} \qquad (\tau = 0), \tag{D5}$$

where the last step follows since we have assumed that the average optical depth is large enough that $P_{rad} \gg F/c$ so that $P_{rad} \simeq P_{rad,iso}$ (note that $P_{rad,iso}$ drops near the hole, but that does not affect the average value of $P_{rad,iso}$ since the hole is small). Combining this result with equation (D1), we write

$$F(\boldsymbol{r}) \simeq \frac{cP_{rad,iso}}{\tau(\boldsymbol{r}) + 4/3} \tag{D6}$$

as an expression that is approximately valid for all τ. With

$$\frac{1}{\bar{\tau}_{eff}} \equiv \frac{1}{A}\int \frac{dA}{\tau(\boldsymbol{r}) + 4/3}, \tag{D7}$$

equation (D2) is valid even if the optical depth is small in some directions. As an example, assume that $\tau = 0$ over an area δA and $\tau = \tau_0 \gg 1$ elsewhere. Then we have

$$\bar{\tau}_{eff} = \frac{\tau_0}{(1 - \delta A/A) + (\delta A/A)[\tau_0/(4/3)]}. \tag{D8}$$

We require $\bar{\tau}_{eff} \gg 1$ in order for our treatment to be valid, and this will be true if both $\tau_0 \gg 1$ and $\delta A/A \ll 1$.

Equations (D1) and (D2) imply that the flux at any point on the shell is then

$$F(\hat{\boldsymbol{r}}) = \frac{\bar{\tau}_{\rm eff}}{\tau(\boldsymbol{r})}\left(\frac{L}{A}\right). \tag{D9}$$

In our problem, $\tau < \bar{\tau}_{\rm eff}$ near the poles, so the flux there is enhanced over L/A since radiation originally directed at regions of high optical depth tends to escape in regions of low optical depth. This is a quantitative expression for the flashlight effect (Yorke & Bodenheimer 1999).

When radiation pressure is acting against gravity, it is convenient to define the critical flux as the flux that just counterbalances gravity,

$$F_{\rm crit} = \frac{Gm_* c}{r^2 \kappa}, \tag{D10}$$

where we have assumed spherical symmetry and where $\kappa = \sigma/\mu$ is the opacity per unit mass and μ is the mean mass per particle. The critical luminosity is then

$$L_{\rm crit} \equiv 4\pi r^2 F_{\rm crit} = \frac{4\pi G m_* \mu c}{\sigma}. \tag{D11}$$

If the opacity is due to electron scattering, the critical luminosity is the Eddington limit. We conclude that supercritical accretion, i.e., accretion when $L > L_{\rm crit}$, can occur in directions with $\tau > \bar{\tau}_{\rm eff}$ since it is possible for F to be less than $F_{\rm crit}$ in those directions:

$$\frac{F(\boldsymbol{r})}{F_{\rm crit}} = \frac{\bar{\tau}_{\rm eff}}{\tau(\boldsymbol{r})}\left(\frac{L}{L_{\rm crit}}\right). \tag{D12}$$

For example, an accretion disk can produce supercritical accretion since the optical depth in the plane of the disk is much larger than that in other directions.

This argument works well in our problem because the Lyα opacity in the central regions is small due to photoionization, thereby rendering the radiation approximately uniform there. It is more difficult to create a uniform radiation field in the case of electron scattering in an ionized gas, since the opacity per unit mass is constant and it is difficult to create a thin, opaque shell around a star. Nonetheless, the effective optical depth in this case is likely to be of order the harmonic mean optical depth, just as we have found for our idealized problem.

APPENDIX E

VERTICAL STRUCTURE OF AN ACCRETION DISK SUPPORTED BY GAS PRESSURE, WITH CONSTANT OPACITY

Here we determine the height of an accretion disk supported by gas pressure under the assumption that the opacity per unit mass, κ, is constant. For a disk supported by gas pressure, the equations describing the radiation field in the disk (see § 6) can be written as

$$\frac{dT^4}{d\Sigma} = \frac{3\kappa F}{4\sigma} \tag{E1}$$

(radiative diffusion), where

$$\Sigma \equiv \int_z^{z_s} \rho\, dz \tag{E2}$$

is the surface density above a height z and

$$\frac{dF}{dz} = \frac{F_0 P}{\int_0^{z_s} P\, dz} \tag{E3}$$

(flux generation). Since gas pressure dominates, we have $P = \rho kT/\mu$, so that this becomes

$$\frac{dF}{d\Sigma} = -\frac{F_0 T}{\Sigma_c \langle T\rangle}, \tag{E4}$$

where $\Sigma_c = \int_0^{z_s} \rho\, dz$ is half the total surface density of the disk and $\langle T\rangle$ is the mass-weighted average temperature in the disk.

To obtain an approximate solution for these two equations, we set

$$T \simeq T_c\left(\frac{\Sigma}{\Sigma_c}\right)^{1/4}\left[\frac{1+\epsilon(\Sigma/\Sigma_c)^{\ell}}{1+\epsilon}\right], \tag{E5}$$

where T_c is the central temperature. The parameters ϵ and ℓ are to be determined; in particular, ϵ is assumed to be small, so that

$$T^4 \simeq T_c^4 \left(\frac{\Sigma}{\Sigma_c}\right) \left[\frac{1+4\epsilon(\Sigma/\Sigma_c)^\ell}{1+4\epsilon}\right]. \tag{E6}$$

Inserting this into equation (E1), we find

$$F = \frac{4\sigma T_c^4}{3\tau_c} \left[\frac{1+4(\ell+1)\epsilon(\Sigma/\Sigma_c)^\ell}{1+4\epsilon}\right], \tag{E7}$$

where $\tau_c \equiv \kappa_R \Sigma_c$ is the optical depth from the midplane to the surface. Since $F = 0$ at the midplane, where $\Sigma = \Sigma_c$, we find

$$\epsilon = -\frac{1}{4(\ell+1)}. \tag{E8}$$

At the surface ($\Sigma = 0$), we have $F = F_0$, so that

$$F_0 = \frac{1}{(1+4\epsilon)} \frac{4\sigma T_c^4}{3\tau_c} \tag{E9}$$

and

$$F = F_0 \left[1 - \left(\frac{\Sigma}{\Sigma_c}\right)^\ell\right]. \tag{E10}$$

Inserting this into equation (E4) and keeping only the leading term in equation (E5) implies $\ell = 5/4$, so that $\epsilon = -\frac{1}{9}$. Since $F_0 = \sigma T_{\rm eff}^4$, equation (E9) implies

$$T_c = \left(\frac{5}{12}\tau_c\right)^{1/4} T_{\rm eff}. \tag{E11}$$

This approach gives a mass-weighted mean temperature $\langle T \rangle = \frac{4}{5} T_c$ from equations (E4) and (E10); on the other hand, direct integration of equation (E5) gives $\langle T \rangle = (17/20) T_c$. The 6% difference between these estimates for $\langle T \rangle$ is a measure of the accuracy of our approximations.

The equation of hydrostatic equilibrium is

$$\frac{dP}{d\Sigma} = \frac{g_0 z}{\varpi}. \tag{E12}$$

Approximating $T \simeq T_c(\Sigma/\Sigma_c)^{1/4}$, which is typically accurate to better than 10%, we then find

$$P = \rho c_{gc}^2 \left(\frac{\Sigma}{\Sigma_c}\right)^{1/4} = \frac{g_0}{\varpi} \int_0^\Sigma z\, d\Sigma'. \tag{E13}$$

Define the characteristic scale height as

$$h_{gc} \equiv \frac{c_{gc}^2}{g_0} = \left(\frac{5\tau_c}{12}\right)^{1/4} \frac{kT_{\rm eff}}{\mu g_0}, \tag{E14}$$

where the second step follows from equation (E11). In terms of the Keplerian velocity $v_K = (g_0 \varpi)^{1/2}$, the scale height is $h_{gc}/\varpi = (c_{gc}/v_K)^2$. Since $\rho = -d\Sigma/dz$, equation (E13) yields the following equation for Σ:

$$\left(\frac{\Sigma}{\Sigma_c}\right)^{1/4} \frac{d\Sigma}{dz} = -\frac{1}{\varpi h_{gc}} \int_0^\Sigma z\, d\Sigma'. \tag{E15}$$

To obtain an approximate solution to this equation, we adopt the following *Ansatz* for Σ:

$$\left(\frac{\Sigma}{\Sigma_c}\right)^{1/4} \simeq \left(1 - \frac{z}{z_s}\right)\left(1 + \frac{z}{2z_s}\right). \tag{E16}$$

An approximate evaluation of the integral $\int z\, d\Sigma'$ gives

$$\int z\, d\Sigma' \simeq z_s \Sigma \left(\frac{1}{3} + \frac{2z}{3z_s}\right). \tag{E17}$$

Integration of equation (E15) then gives

$$\left(\frac{\Sigma}{\Sigma_c}\right)^{1/4} \simeq \frac{z_s^2}{6\varpi h_{gc}} \left(1 - \frac{z}{z_s}\right)\left(1 + \frac{z}{2z_s}\right), \tag{E18}$$

which is consistent with the *Ansatz* provided that the height of the disk is

$$z_{sg} = \left(6\varpi h_{gc}\right)^{1/2}, \tag{E19}$$

where the subscript g indicates that the height is evaluated for the case in which gas pressure dominates. Shakura & Sunyaev (1973) show that the height of the disk is $\sim(c_c/v_{\rm K})\varpi$, where c_c is the central isothermal sound speed. Equation (E19) implies that in a gas pressure–dominated disk,

$$\frac{z_{sg}}{\varpi} = \frac{\sqrt{6} c_{gc}}{v_{\rm K}}. \tag{E20}$$

In terms of the sound speed at the photosphere, $c_{g,\rm eff} = (kT_{\rm eff}/\mu)^{1/2}$, this is

$$\frac{z_{sg}}{\varpi} = (540\tau_c)^{1/8} \frac{c_{g,\rm eff}}{v_{\rm K}}. \tag{E21}$$

Numerical integration of the structure equations shows that the actual height of a gas pressure–dominated disk ranges from $1.04 z_{sg}$ for $\tau_c = 10^4$ to $1.10 z_{sg}$ for $\tau_c = 10^9$, so the approximations made in our analytic estimate are reasonably good.

Paczyński & Bisnovati-Kogan (1981) obtained equation (E20) through a different argument: they assumed that the disk is polytropic, with $P \propto \rho^{1+1/n}$, and found that

$$\frac{z_{sg}}{r} = \frac{[2(n+1)]^{1/2} c_{gc}}{v_{\rm K}}. \tag{E22}$$

They argued that n is likely to be between 1.5 and 3, so that $2(n+1)$ is between 5 and 8; they chose 6 as a typical value. We emphasize that our derivation depends only on the assumption that the opacity is constant and is not based on the assumption that the gas is polytropic.

To complete the determination of the height of a gas pressure–supported disk, we must estimate the optical depth through half the disk, $\tau_c = \kappa_{\rm R}\Sigma_c$. Observe that

$$\int_0^{z_s} P\, dz = \int_0^{z_s} \left(\frac{kT}{\mu}\right) d\Sigma \simeq \left(\frac{k\langle T\rangle}{\mu_c}\right)\Sigma_c, \tag{E23}$$

where μ_c is the central value of the mean molecular weight. According to the discussion below equation (E11), the average temperature is $\langle T\rangle \simeq \frac{4}{5} T_c$, and we adopt this value here. The fact that $\langle T\rangle$ is so close to T_c justifies setting the mean molecular weight equal to μ_c, as we have done. From equation (52), we then find

$$\tau_c = \frac{\Omega \kappa_{\rm R} \dot{m}_* f}{6\pi\alpha[(4/5)kT_c/\mu_c]}. \tag{E24}$$

Equation (E11) then implies

$$\frac{T_c}{T_{\rm eff}} = \left[\frac{25\Omega\kappa_{\rm R} f}{288\pi\alpha(kT_{\rm eff}/\mu_c)}\right]^{1/5}. \tag{E25}$$

Using this result in equation (E20) for the height of a gas pressure–supported disk, we find

$$z_{sg} = 1.21\times 10^{10} \left(\frac{\phi_I \kappa_{\rm R}}{\alpha_{-2}\kappa_{\rm T}}\right)^{1/10} \left(\frac{\varpi}{R_\odot}\right)^{21/20} \frac{\left(\dot{m}_{*,-3} f\right)^{1/5}}{m_{*,2}^{7/20}} \ {\rm cm}, \tag{E26}$$

where we have normalized α to a typical value of 0.01.

REFERENCES

Abel, T., Bryan, G. L, & Norman, M. L. 2002, Science, 295, 93 (ABN02)
Adams, T. F. 1972, ApJ, 174, 439
Ahn, K., & Shapiro, P. R. 2007, MNRAS, 375, 881
Artemova, I. V., Bisnovatyi-Kogan, G. S., Bjoernsson, G., & Novikov, I. D. 1996, ApJ, 456, 119
Balbus, S. A., & Hawley, J. F. 1998, Rev. Mod. Phys., 70, 1
Beers, T. C., & Christlieb, N. 2005, ARA&A, 43, 531
Begelman, M. C., McKee, C. F., & Shields, G. A. 1983, ApJ, 271, 70
Bromm, V., Coppi, P. S., & Larson, R. B. 1999, ApJ, 527, L5
———. 2002, ApJ, 564, 23
Bromm, V., Kudritski, R. P., & Loeb, A. 2001, ApJ, 552, 464
Bromm, V., & Larson, R. B. 2004, ARA&A, 42, 79
Bromm, V., & Loeb, A. 2003, Nature, 425, 812
———. 2004, NewA, 9, 353
Clark, P. C., Glover, S. C. O., & Klessen, R. S. 2008, ApJ, 672, 757
Daigne, F., Olive, K. A., Vangioni-Flam, E., Silk, J., & Audouze, J. 2004, ApJ, 617, 693
D'Alessio, P., Canto, J., Calvet, N., & Lizano, S. 1998, ApJ, 500, 411
Elmegreen, B. G. 1997, ApJ, 486, 944
Fatuzzo, M., Adams, F. C., & Myers, P. C. 2004, ApJ, 615, 813
Figer, D. F. 2005, Nature, 434, 192
Frank, J., King, A., & Raine, D. 1995, Accretion Power in Astrophysics (2nd ed.; Cambridge: Cambridge Univ. Press)
Giroux, M. L., & Shapiro, P. R. 1996, ApJS, 102, 191
Glover, S. C. O., & Brand, P. W. J. L. 2001, MNRAS, 321, 385
Gradshteyn, I. S., & Ryzhik, I. M. 1965, Table of Integrals, Series and Products (New York: Academic)
Greif, T. H., & Bromm, V. 2006, MNRAS, 373, 128
Haehnelt, M. G. 1995, MNRAS, 273, 249
Harrington, J. P. 1973, MNRAS, 162, 43
Heger, A., & Woosley, S. E. 2002, ApJ, 567, 532
Hollenbach, D., Johnstone, D., Lizano, S., & Shu, F. 1994, ApJ, 428, 654
Hummer, D. G., & Kunasz, P. B. 1980, ApJ, 236, 609
Hunter, C. 1977, ApJ, 218, 834
Iglesias, C. A., & Rogers, F. J. 1996, ApJ, 464, 943
Ivanov, V. V. 1970, Astrophysics, 6, 355
Jackson, J. D. 1975, Classical Electrodynamics (New York: Wiley)
Jappsen, A.-K., Klessen, R. S., Glover, S. C. O., & Mac Low, M.-M. 2007, ApJ, submitted (arXiv:0709.3530)
Jijina, J., & Adams, F. C. 1996, ApJ, 462, 874
Krumholz, M. R., Klein, R. I., & McKee, C. F. 2005a, in Massive Star Birth: A Crossroads of Astrophysics, ed. R. Cesaroni et al. (Cambridge: Cambridge Univ. Press), 231
Krumholz, M. R., McKee, C. F., & Klein, R. I. 2005b, ApJ, 618, L33
Kudritzki, R. 2002, ApJ, 577, 389
Larson, R. B. 1969, MNRAS, 145, 271
Larson, R. B., & Starrfield, S. 1971, A&A, 13, 190
Matzner, C. D., & McKee, C. F. 2000, ApJ, 545, 364
McKee, C. F., & Holliman, J. H. 1999, ApJ, 522, 313
McKee, C. F., & Tan, J. C. 2002, Nature, 416, 59
———. 2003, ApJ, 585, 850
Meyer, F., & Meyer-Hofmeister, E. 1982, A&A, 106, 34
Meynet, G., Ekström, S., & Maeder, A. 2006, A&A, 447, 623
Nakano, T., Hasegawa, T., & Norman, C. 1995, ApJ, 450, 183
Neufeld, D. A. 1990, ApJ, 350, 216
Norman, M. L., O'Shea, B. W., & Paschos, P. 2004, ApJ, 601, L115
Oh, S. P., & Haiman, Z. 2002, ApJ, 569, 558
Ohkubo, T., Umeda, H., Maeda, K., Nomoto, K., Suzuki, T., Tsuruta, S., & Rees, M. J. 2006, ApJ, 645, 1352
Omukai, K., & Inutsuka, S. 2002, MNRAS, 332, 59
Omukai, K., & Nishi, R. 1998, ApJ, 508, 141
———. 1999, ApJ, 518, 64
Omukai, K., & Palla, F. 2001, ApJ, 561, L55
———. 2003, ApJ, 589, 677
Omukai, K., Tsuribe, T., Schneider, R., & Ferrara, A. 2005, ApJ, 626, 627
O'Shea, B. W., McKee, C. F., Heger, A., & Abel, T. 2008, in The First Stars III, ed. B. W. O'Shea, A. Heger, & T. Abel, in press
O'Shea, B. W., & Norman, M. L. 2007, ApJ, 654, 66
Osterbrock, D. E. 1989, Astrophysics of Gaseous Nebulae and Active Galactic Nuclei (Mill Valley: University Science Books)
Paczyński, B., & Bisnovati-Kogan, G. 1981, Acta Astron., 31, 283
Padoan, P., & Nordlund, A. 2002, ApJ, 576, 870
Penston, M. V. 1969, MNRAS, 144, 425
Ripamonti, E., & Abel, T. 2004, MNRAS, 348, 1019
Ripamonti, E., Haardt, F., Ferrara, A., & Colpi, M. 2002, MNRAS, 334, 401
Scannapieco, E., Kawata, D., Brook, C. B., Schneider, R., Ferrara, A., & Gibson, B. K. 2006, ApJ, 653, 285
Schaerer, D. 2002, A&A, 382, 28
Schaye, J., Aguirre, A., Kim, T.-S., Theuns, T., Rauch, M., & Sargent, W. L. W. 2003, ApJ, 596, 768
Shakura, N. I., & Sunyaev, R. A. 1973, A&A, 24, 337
Shapiro, P. R., Iliev, I. T., & Raga, A. C. 2004, MNRAS, 348, 753
Shapiro, S. L., & Teukolsky, S. A. 1983, Black Holes, White Dwarfs, and Neutron Stars (New York: Wiley)
Shu, F. H. 1977, ApJ, 214, 488
———. 1991, The Physics of Astrophysics, Vol. I: Radiation (Mill Valley: University Science Books)
———. 1992, The Physics of Astrophysics, Vol. II: Gas Dynamics (Mill Valley: University Science Books)
Spitzer, L., Jr. 1978, Physical Processes in the Interstellar Medium (New York: Wiley)
Stahler, S. W., Palla, F., & Salpeter, E. E. 1986, ApJ, 302, 590
Susa, H. 2007, ApJ, 659, 908
Tan, J. C., & Blackman, E. G. 2004, ApJ, 603, 401
Tan, J. C., & McKee, C. F. 2004, ApJ, 603, 383 (Paper I)
———. 2008, in The First Stars III, ed. B. W. O'Shea, A. Heger, & T. Abel, in press (arXiv:0711.4116)
Tarter, C. B., & McKee, C. F. 1973, ApJ, 186, L63
Tegmark, M., Silk, J., Rees, M. J., Blanchard, A., Abel, T., & Palla, F. 1997, ApJ, 474, 1
Terebey, S., Shu, F. H., & Cassen, P. 1984, ApJ, 286, 529
Tumlinson, J. 2006, ApJ, 641, 1
Tumlinson, J., & Shull, J. M. 2000, ApJ, 528, L65
Tumlinson, J., Venkatesan, A., & Shull, J. M. 2004, ApJ, 612, 602
Uehara, H., & Inutsuka, S.-i. 2000, ApJ, 531, L91
Ulrich, R. K. 1976, ApJ, 210, 377
Whalen, D., O'Shea, B. W., Smidt, J., & Norman, M. L. 2008, ApJ, submitted (arXiv:0708.3466)
Woods, D. T., Klein, R. I., Castor, J. I., McKee, C. F., & Bell, J. B. 1996, ApJ, 461, 767
Yorke, H. W., & Bodenheimer, P. 1999, ApJ, 525, 330
Yorke, H. W., & Sonnhalter, C. 2002, ApJ, 569, 846
Yoshida, N., Omukai, K., Hernquist, L., & Abel, T. 2006, ApJ, 652, 6